University Hospital Zurich
Division of Cardiac and Vascular Surgery
Head of Division: Prof. Volkmar Falk, MD

Supervision by
Prof. Simon P. Hoerstrup, MD, PhD
Dr. sc. nat. Jens M. Kelm

Aging and Remodeling Processes of Tissue Engineered Pulmonary Arteries in a Growing Sheep Model

INAUGURAL-DISSERTATION
zur Erlangung der Doktorwürde der Medizinischen Fakultät
der Universität Zürich

vorgelegt von

Armin Andreas Zürcher
von Zürich und Menzingen, ZG

Genehmigt auf Antrag von Prof. Dr. med. S.P. Hoerstrup
Zürich 2010

Table of Contents

1 Abstract

1.1 Aim of the Study

Living tissue engineered vascular grafts are a next generation treatment for arterial replacements with enormous potential. However, despite promising preclinical trials, there is currently no information available on how biological age of the implanted graft compares to the corresponding native artery. Major remodelling processes and maturation of tissue engineered arteries have been observed in vivo, especially in regard to cell number and extracellular matrix, but only little is known about the origin of these cells, the driving forces behind the remodelling process and their impact on graft functionality and survival. However, clarification of the mechanisms of tissue/cellular remodelling processes is critical for future clinical implementation of cardiovascular grafts.

Analyzing a 240 weeks follow-up sheep study with implanted tissue engineered pulmonary arteries provided the opportunity to compare the cellular age of tissue engineered cardiovascular constructs and their native counterparts focusing on telomere length as a renowned endogenous marker linked to cellular and organismal aging.

1.2 Methods and Results

Relative telomere length and telomerase activity were determined of serially passaged vascular myofibroblasts harvested from the external jugular and saphenous veins of three Swiss Alpine Lambs. Quantitative telomere length analysis (Q-FISH) and immunohistological analyses were conducted in explanted pulmonary artery grafts fabricated from biodegradable scaffold material seeded with autologous vascular cells 5, 20, 50, 100 and 240 weeks post implantation.

The results show strong evidence that the cell age of tissue engineered pulmonary arteries is significantly lower than in their native counterparts. Furthermore, histological analyses provide important cues on the basic remodelling processes of a tissue-engineered graft.

1.3 Conclusion

This study provides evidence that telomere length may be used to assess cellular age in tissue engineered vascular grafts. Remodeling processes are crucial to ensure growth and graft functionality in a growing sheep model and may be, in combination with the in vitro graft production conditions, at the cost of premature aging.

2 Introduction

2.1 Rationale of Tissue Engineering

The concept of tissue engineering is an integrative part of regenerative cardiovascular medicine and offers an alternative approach to current treatment strategies in a variety of cardiovascular disorders such as congenital or acquired complex heart diseases or peripheral arterial disease [1,2]. With stem cell based therapies continuously gaining attention, the concept has also been introduced to the treatment of myocardial infarction and severe heart failure [3,4]. One of the major motivations is substantiated by the replacement of compromised biological structures for which the use of today's "conventional" non-biodegradable grafts is limited for example due to their inability to adapt to growth and development of the target structure. Tissue engineering aims to replace dysfunctional tissues by using an in vitro generated fully functional living construct containing cells, ideally of autologous origin, in combination with biodegradable scaffold materials [5]. Key characteristics of these constructs are their potential to undergo self-renewal, healing and remodeling processes post implantation [1,6]. However, several aspects such as the individual contribution of these processes to long-term integration and aging of a tissue-engineered vascular graft (TEVG) are poorly understood and need to be addressed in order to further improve graft quality and fabrication processes and to facilitate the design of biologically dynamic scaffold materials.

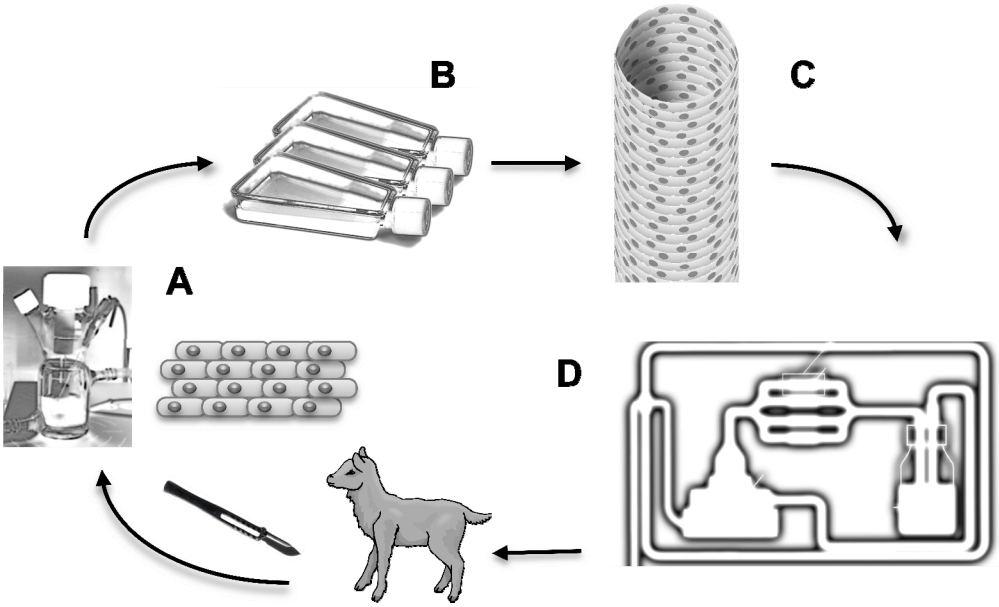

Figure 1: **Design of a tissue engineered vascular graft (TEVG). [A] Tissue or cells are harvested from the host/donor animal, isolated and prepared for cultivation. [B] After the expansion phase to obtain sufficient cell numbers, the cells are seeded onto biodegradable scaffolds [C] Tissue maturation and conditioning is achieved using a pulsatile flow/pressure system [D] mimicking an in vivo environment before implanting the TEVG into the host animal.**

2.2 Graft remodeling – What happens to the cells?

Several studies addressing remodeling processes in tissue engineered cardiovascular grafts have been published. Stock et al. [7] used poly-4-hydroxybutyric acid patches seeded with autologous cells transgenic for green fluorescence protein (GFP) for pulmonary artery augmentation in a lamb model. The results demonstrated an increased DNA content of the seeded patches until day 49 of the implantation period, suggesting an increase of the total cell number within the graft. In addition, ingrowth of native cells into an unseeded control patch from its surroundings after an implantation period of 140 days has been observed. Data presented by Matsumura et al. [8] imply that canine bone marrow cells (BMC) initially seeded onto a co-polymeric scaffold and circulating endothelial cells contribute to histogenesis of a vascular autograft. BMCs were labeled with carboxyfluorescein diacetate succinimidyl ester (CFDA-SE) before seeding and could be followed up until eight weeks post implantation. Further investigation of transplanted pulmonary artery patches by Mettler

et al. [9] consisted of green and red fluorescent protein (GFP and RFP, respectively) retrovirally labeled endothelial progenitor and mesenchymal stem cells as a cell source. He reported a cellular persistence of 66% after 6 weeks by measuring immunofluorescent signals of seeded GFP and RFP transduced cells.

There is only limited information available regarding results on long-term remodeling processes. However, understanding of these processes is mandatory for any future clinical application to ensure graft durability, ideally over a patient's lifetime. In accordance to the results of Stock et al., Hoerstrup and coworkers demonstrated an approximately fivefold increase in the DNA content, comparing a pulmonary vascular graft prior to implantation and at 100 weeks post implantation, reaching similar DNA amounts compared to native pulmonary artery [6]. Three mechanisms are proposed to contribute to the remodeling processes: (i) proliferation and differentiation of the cells used to produce the graft [8,10], (ii) cell migration from adjacent tissue [9-12] and (iii) recruitment of circulating progenitor cells [9, 12].

2.3 Technologies to monitor cell remodeling processes

Various labeling techniques have been developed to monitor and identify remodeling processes on a cellular level. These include genetic markers such as sex-mismatched donor-host systems, fluorescent organic dyes, nanoparticles such as carbon nanotubes, magnetodendrimers and quantum dots and transgenic labeling such as viral transduction or transfection with reporter genes (LacZ, GFP, norepinephrine transporter, sodium-iodide symporter). Due to their individual properties and labeling mechanisms, they provide an enormous tool box for tissue engineering purposes and can be tailored to particular needs.

2.3.1 Cell labeling

Many cell labeling techniques available today present a valuable tool to assess cellular fate. The fact that they are all artificially introduced or added to viable cells which in some cases adversely affects cell functionality is one of their common undesirable features [13].

Moreover, cell labeling requires a substantial amount of time or extensive preparation of cell populations before they are accessible to analyses, especially if large numbers of cells are required to produce the tissue engineered construct. We therefore sought for an endogenous marker which could complement available techniques and provide information even in long term studies of more than 20 weeks which has thus far been a mutual shortcoming of most cell labeling methods. Telomere length may serve as such an endogenous marker due to the fact that in many settings, cells intended for seeding of tissue engineered grafts undergo a considerable number of population doublings before a sufficient amount of cells is reached.

2.3.1.1 Fluorescent dyes

Fluorescent dyes may be divided into several categories depending on their mechanism of staining [14]. (i) DNA-binding fluorescent dyes such as HOECHST 33342 and thiazole orange can be used for cell tracking in vivo up to several days but are inhibiting cell functions. (ii) Cytoplasmatic fluorescent dyes contain esterase sensitive sidechains which allows trapping of these molecules after membrane permeation. Calcein is well-known representative of this group and has been used for short duration in vivo lymphocyte migration studies [15]. (iii) Covalent coupling fluorescent dyes are characterized by high membrane permeability and subsequent coupling with intracellular molecules. In the case of CFDA-SE, cell labeling could be observed for up to 8 weeks [16].

2.3.1.2 Retroviral transduced reporter genes

Transgenic technologies are meanwhile laboratory routine to label cells with fluorescence proteins such as enhanced yellow fluorescent protein (EYFP), GFP or RFP. However, these technologies are rather suited for small animal trials with low amount of cells required. Moreover, disappearance of the fluorescent signal can be either due to cell death, wash out during proliferation or gene silencing [17].

2.4 Magnetic resonance imaging

Magnetic resonance imaging (MRI) offers a potent and particularly non-invasive tool to monitor processes in vivo. To generate sufficient MR contrast, cells can be labeled with supraparamagnetic iron oxides encapsulated in repeatedly branched molecules called carboxylated polyamidoamine dendrimers [18]. These magnetodendrimers allow non-specific and non-receptor mediated uptake and accumulation in cells and have been used to monitor muscle stem cell transfer in mice over a 14-day period [19]. In T2 and T1 weighed images, results show well-defined areas of decreased signal intensity corresponding to the correct location of the transferred stem cells in comparison with conventional histological analysis. Viability, proliferation and differentiation of labeled cells were reported to be similar to non-labeled cells.

However, reported by Terrovitis et al. [20] this method is indeed useful for localizing the anatomic site of cardiac stem cell transfer but it is not reliable for monitoring long-term cell viability, as the acquired signals may also originate from dead cells and from macrophages which have taken up the ferrum oxide particles.

2.4.1.1 Carbon nanotubes and quantum dots

The platform technology of carbon nanotubes is continuously on the rise for tissue engineering purposes since the discovery by Iijima et al. [21]. Nanotubes consist of a cylindrical structure with diameters in nanometer dimension and are multifunctional in terms of their individual structural and electronic properties defined by length, diameter and chirality [22]. Optical labeling of fibroblasts and murine myoblast stem cells by ingested single-walled carbon nanotubes was demonstrated in experiments by Heller et al [23]. By functionalizing nanotubes with gadolinium (termed gadonanotubes), this technology could be made accessible for MRI imaging, which due to their high contrast ability, offers future possibilities for monitoring engineered tissues [22, 24].

Quantum dots are semiconductor nanocrystals with highly photostable characteristics. They have been proposed as an alternative to the conventionally used fluorophores for cell labeling. Experiments by Jaiswal et al. [25] showed that HeLa cells could be stably labeled with quantum dots over a week. He reported no interference in growth or differentiation of the cells. Using quantum dot antibody bioconjugates, the possibility exists to specifically label the cell type of interest. Quantum dots have overcome some of the shortcomings of fluorescent dies, such as their limited absorption range, their broad emission spectra and their vulnerability to photobleaching effects. However, quantum dots still have a limited lifetime in aqueous solutions [23]. In addition, quantum dot cores consist of semiconductor metals (CdS, CdSe, CdTe, ZnS, PbS) which may have cytotoxic effects when exposed to cellular components [23,26].

2.4.1.2 Host-Donor Sex Mismatch

A sex mismatched model offers a very reliable technique to monitor cellular remodeling processes. Location of the Y-chromosome can be determined by fluorescence in situ hybridization using a DNA-probe [27,28]. It is not subject to washout or loss of signal strength. However, it is by definition not suitable in an autologous setting.

2.5 Cell Aging

The aforementioned labeling technologies have been successfully used in small and large animal trials. Sex mismatch is the most reliable marker to evaluate cell graft persistence. However, these technologies are hardly applicable for autologous long term preclinical animal model systems since the ideal marker is not subject to any artificial or transient labeling technique, respectively, and does not require nanoparticles or transgenic technologies which may hamper native cell phenotype and may lead to false positive signals. Therefore, we have decided to analyze telomere lengths to investigate aging effects and its suitability as an endogenous marker in long term animal trials.

2.5.1 Telomeres and telomere length

Any cell with a linear genome uses RNA primers to initiate DNA replication at the lagging DNA strand. Removal of the RNA primer at the end of the lagging strand leaves a single strand overhang of unreplicated DNA. Due to the fact that the DNA replication process is semi-conservative and unidirectional in its nature, the inability to replicate this last piece of DNA has been termed the end-replication problem since polymerases cannot initiate the formation of DNA on a template de novo. Without protective measures, this would eventually lead to the loss of terminal sequences by enzymatic degradation and end-to-end fusions of chromosomes or activation of DNA repair mechanisms. In 1973, the end-replication problem served Olovnikov as an explanation for the limited cell doubling potential of normal somatic cells in his theory of marginotomy [29] and by the 1980s, the molecular structure of the telomeric region of chromosomes has been identified [30,31].

Telomeres are repeated DNA-Sequences $(5'\text{-TTAGGG-}3')_n$ capping the end of chromosomes. In association with several proteins, the telomere system forms a t-loop [32, 33], which provides protection against chromosomal instability and DNA damage response (DDR) pathways. The length of the telomeric repeats, measured as lengths of terminal restriction fragments (TRF, HinfI/RsaI) ranges from 6-7kbp in dermal fibroblasts [34], 9-12kbp in endothelial cells of the internal thoracic artery (age-dependent) [35], 12-21kbp in ovine skin fibroblasts derived from 1-36 month old animals [36] to 5-12kbp in peripheral blood leukocytes [37] in humans and is highly variable among individuals. The observed range may be detectable as early as in the germline with reported variable telomere lengths of human semen samples ranging from less than 9 to over 17kb [38]. Furthermore, telomere length may at least partly be an inherited trait as described by Jesper et al. [39].

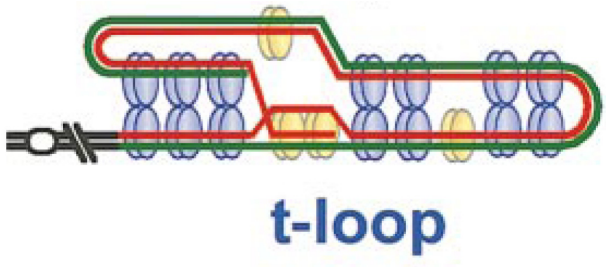

Figure 2: T-Loop structure of the telomeric region (adapted from Griffith et al. [33]). The blue and yellow ovals depict TRF1 and TRF2 (telomeric repeat–binding factors 1 and 2, respectively), providing a protective mechanism for the telomeric ends. The red string shows the $[TTAGGG]_n$ sequence, in green $[CCCTAA]_n$, and in black the non-telomeric DNA.

2.5.2 Cellular Senescence

Based on the theory of marginotomy by Olovnikov et al. in 1973 [29], telomeres have been described as the internal “mitotic clock” of cells. The erosion of telomeric sequences with each cell division may eventually lead to a critical telomere length, which in return leads to a p53-dependent growth arrest. This process was first described by Hayflick et al. [40], who observed that this growth arrest occurred after a specific number of cell divisions in human diploid cell strains, which was termed the “hayflick limit”. This phenomenon later became one of the cornerstones of the theory of replicative scenescence [41]. Groundwork for this theory has also been laid by Wright et al. which, based on the results of in their experiments with SV40 (Simian vacuolating virus 40) transfected humand diploid fibroblasts, proposed a two-stage model for cellular scenescence [42]. The first stage termed Mortality Stage I represents a p53-dependent arrest in phase G1/S of the cell cycle. Notably, Greider et al. found that the initial length of telomeric terminal restriction fragments is directly proportional to the replicative capacity of a cell line [43] and thus supporting the concept of replicative senescence in accordance with Choudhury et al., who showed that the p53/23 induced cell cycle arrest is activated by telomere shortening and dysfunction [44]. The second stage (Mortality Stage II), in an attempt to undergo cell division, leads to a cellular crisis characterized by extensive telomere dysfunction and chromosomal instability leading to cell death [45].

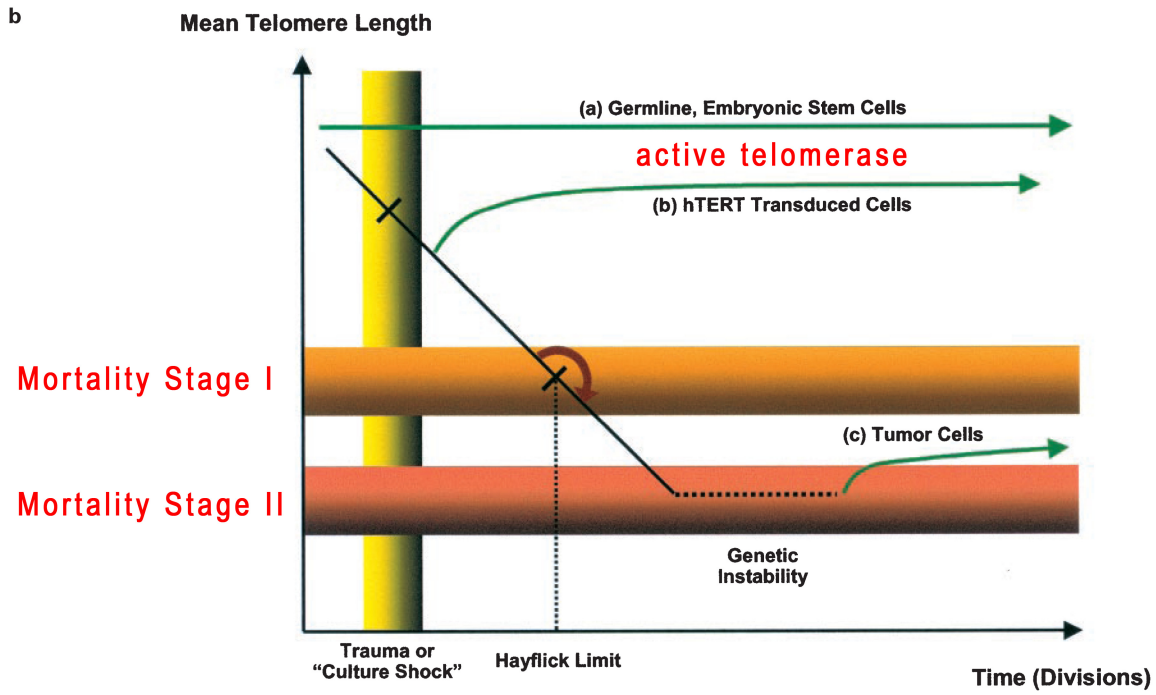

Figure 3: Mortality Stage I and II in cellular senescence. The concept of cellular senescence illustrated by a gradual decrease of telomere length during cell replication (divisions). Two mechanisms, either by artificially inducing active telomerase (b) or by overcoming a p53-dependent cell cycle arrest (curved brown arrow), are shown to escape Mortality Stage I, possibly leading to the formation of tumor cells (c). (a) shows cells with active telomerase, which do not undergo telomere shortening. Figure adapted from Harley et al. [46]

2.5.3 Telomerase

Cells without limitations in their replicative capacity such as tumor cell lines or embryonic stem cells are obviously in need of a mechanism which can escape the status of cellular senescence. A specific telomere terminal transferase (termed telomerase) adds tandem [TTGGGG] repeats onto synthetic telomere primers in yeasts maintaining the telomeric region despite continuous cell divisions [47]. Further investigation showed that the active enzyme telomerase is a ribonucleoprotein containing two subunits, the catalytic subunit hTERT (human telomerase reverse transcriptase) and the template-containing RNA subunit hTR (human telomerase RNA). Telomerase or its catalytic subunit, respectively, is expressed in approximately 98% of immortal cell lines [48], germ cell lines and many types of tumors. However, telomerase is not an oncogene as telomerase activity does not necessarily lead to

loss of growth control, a process which needs to be clearly separated from cell immortalization as it is seen in human embryonic stem cells [49] or germline cells.

2.6 Scaffold material

For most applications, a suitable scaffold material for generating a graft that measures up to the demands and conditions of an in vivo tissue-specific environment is required. The prerequisites are extensive and should feature structural properties similar to natural extracellular matrix. For vascular tissue engineering, polymeric scaffold materials are mainly used due to their favorable properties. With the improvement of production techniques, such as electrospinning to create polymeric nanofibers [50,51], there is a trend to further functionalize scaffold materials based on nanotechnology as it is the case with the incorporation of drug-delivery vehicles in biodegradable polymeric scaffolds [52].

Table 1: Basic characteristics of an ideal tissue scaffold, adapted from Murugan et al. [53]

Characteristics	General remarks
Biocompatible	Biologically compatible to host tissue (i.e., should not provoke any rejection, inflammation, and immune responses)
Biodegradable	The rate of degradation must perfectly match the rate of tissue regeneration, and the degraded product(s) should not harm the living tissues
Vascular supportive	Should provide channels for blood supply for fast and healthy tissue regeneration
Nontoxic	Should not evoke toxicity to tissues
Nonimmunogenic	Should not evoke immunogenic response to tissues
Noncorrosive	Should not corrode at physiological pH and at body temperature
Porosity with interconnected pores	To maximize the space for cellular adhesion, growth, extra-cellular matrix secretion, revascularization, adequate nutrition and oxygen supply without compromising mechanical strength
3D structure	To assist cellular ingrowth and transport of nutrients and oxygen
High surface area to volume ratio	To accommodate high-density cells
Surface modifiable	To functionalize chemical or biomolecular groups to improve cell adhesion
Adequate mechanical strength	To withstand in vivo stimuli
Sterilizable	To avoid toxic contamination

2.7 Working hypothesis and study outline

Caused by tissue remodeling and growth processes and the accelerated expansion phase in vitro to produce a sufficient amount of cells for of a tissue engineered vascular graft, we hypothesize that there is a significant difference in the biological age of the tissue-engineered vascular grafts compared to their native counterparts.

To validate the reduction in telomere length during cell expansion, myofibroblasts were isolated from the external jugular and great saphenous vein of three Swiss White Alpine lambs. The cells were serially passaged and relative telomere length of cultured cells measured by Flow-FISH (fluorescent in-situ hybridization) analysis. The absence of telomerase activity of the isolated cell populations were confirmed by a telomere repeat amplification protocol (TRAP).

To investigate the age of native and tissue engineered blood vessels, explant specimens of TEVG 5, 20, 50, 100 and 240 weeks post-implantation in an growing sheep model were evaluated using Q-FISH (quantitative fluorescent in-situ hybridization) analysis.

Furthermore, immunohistological analysis of the tissue engineered implants at the site of anastomosis to further unravel the cellular remodeling mechanisms have been performed.

3 Material and Methods

3.1 Blood vessel tissue engineering and implantation

Generation and implantation of tissue engineered pulmonary arteries in a growing sheep model was performed earlier by Hoerstrup and coworkers. Briefly, endothelial cells were obtained from segments of carotid artery and jugular vein derived from Swiss White Alpine lambs (age: 44±2 days, weight: 15.58±5.55 kg, n=6) using collagenase digestion [6]. Myofibroblasts were extracted from the remaining de-endothelialized vessel segments and used after about 16 doubling times (average doubling time: 28.3 h ± 6.6 h, n=6). The expanded myofibroblasts were seeded in three fractions onto PGA/P4HB composite arterial scaffolds (18 mm ± 1 mm) in 24h intervals (4.5E6 to 5.5E6 cells per cm^2) under static culture conditions using Dulbecco's modified Eagle's medium (DMEM, Invitrogen, Carlsbad, CA) supplemented with 10% lamb serum (GibcoBRL; Cat. No. 16070096, Lot. No. 6050576D). Thereafter, the conduits were covered with endothelial cells (1E6 per cm^2). After additional three days grown under static culture conditions, the vascular grafts were placed into a pulse duplicator bioreactor system [6], and grown under gradually increasing flow conditions (50 mL/min to 550 mL/min, 1Hz) for 14 days. The culture medium was changed every three to four days. The tissue engineered vascular grafts were implanted into lambs (n = 6, 165±46 days old, 27.33±3.84 kg). The heart was exposed by a left anterolateral thoracotomy through the third intercostal space. Cardio-pulmonary bypass was performed via right femoral artery and right atrial cannulation. Following exposure and mobilisation of the main pulmonary artery, approximately 2cm of native pulmonary artery was excised. Experimental duration was up to 240 weeks, representing the full biological growth cycle of this animal model. Animals included in this study were analyzed after 5, 20, 50, 100 and 240 weeks post mortem.

3.2 Ovine cell isolation and culture

Segments of 3-4cm in length of the external jugular vein (OVJ) and the great saphenous vein (OVS) of three Swiss White alpine lambs aged 4-6 months were harvested and transferred to the lab on ice immediately. The pieces were washed in PBS (Kantonsapotheke, Zurich, Switzerland), manually stripped of the surrounding adventitial tissue and minced into small pieces of approximately 2-3mm. Collagenase digestion was conducted using DMEM medium (Gibco, Invitrogen, CA, USA) supplemented with 2ug/ml of Collagenase A (Roche Diagnostics GmbH, Switzerland) and 5% 1M Hepes buffer (Gibco). The solution was incubated for 2h in a humidified atmosphere at 37°C containing 5% CO2. A magnetic stirrer was used to ameliorate separation of the cells mechanically. The cell suspension was then strained (Falcon 20µm cell strainer) and transferred to a cell culture flask. The isolated cells were expanded as monolayer cultures in DMEM supplemented with 10% Lamb Serum (Gibco), 2mM Glutamax (Gibco) and 1% Penicillin/Streptpmycin (Gibco). Medium was exchanged every 3 days and cell cultures split at subconfluency at a ratio of approximately 1:4. Cells were cryopreserved in liquid nitrogen at -196°C using Lamb Serum (Gibco) and 10% DMSO Hybri-Max (Sigma) until further use.

3.3 Flow-FISH (fluorescent in-situ hybridization)

Relative telomere length was measured according to the manufacturer's protocol for Flow-FISH analysis (Telomere PNA Kit/FITC, Dako, Glostrup, Denmark). Briefly, DNA of cryopreserved ovine external jugular and great saphenous vein myofibroblasts was denaturized for 15min at 82°C and hybridized using a ready-to-use hybridization solution (DakoCytomaton) containing 70% formamide for non-stained cell samples and a FITC-conjugated PNA telomere probe targeted to the repetitive telomere sequence $[TTAGGG]_n$, respectively. The hybridization (overnight in the dark at room temperature) was followed by washing twice with a wash solution for 10min at 40°C. After washing, the samples were resuspended in DNA-staining solution containing propidium iodide (PI) and RNase A. After incubation of a minimum of 2 hours at 4°C, samples were measured using a fluorescent cell

sorter (FACS Calibur, BD Biosciences, Belgium) and analyzed with FlowJo software Version 7.5 (Tree Star Inc, Ashland, Oregon, USA). PI was used to gate only for the cells which are in G0/G1 cell cycle state. As control cell line, we used the tetraploid human T cell line 1301, a sub-line of the EBV genome negative T-cell leukaemia line [54] obtained from Interlab Cell Line Collection (IST), Genova, Italy. The ratio between the mean fluorescence intensity (MFI) of the myofibroblasts and the control cell line is expressed as the relative telomere length (RTL), calculated as:

$$\mathrm{RTL} = 100 \times \frac{(\mathrm{MFI}_{\text{MF with PNA}} - \mathrm{MFI}_{\text{MF without PNA}}) \times 2_{\text{DNA Index 1301}}}{\mathrm{MFI}_{\text{1301 with PNA}} - \mathrm{MFI}_{\text{1301 Without PNA}}}$$ whereas PNA signal is represented in the

FL-1 channel and PI in the FL-3 channel.

3.4 Telomerase Activity (TRAP and ELISA)

Telomerase activity was measured using the TRAP telomeric repeat amplification protocol according to the kit's manufacturer (*Telo*TAGGG Telomerase PCR ELISA, Roche Diagnostics GmbH, Switzerland). Cell pellets consisting of 2x10E5 cells were stored at -80°C until performing the assay. The samples were resuspended in lysis reagent (Roche Diagnostics) and incubated on ice for 30min before the lysate was centrifuged at 4°C and 16000xG for 20min before performing the TRAP reaction. To create negative controls, cell extracts were heat-treated for 10min at 85°C prior to the TRAP reaction. 3µl of the cell extracts, the positive controls supplied by the manufacturer and the reaction mixture (Roche Diagnostics) containing telomerase substrate, primers, nucleotides and Taq polymerase were transferred to Eppendorf tubes suitable for PCR amplification. The amplification was carried out using an Eppendorf Mastercycler (Eppendorf, Netheler, Germany). The elongation of a biotin-labeled synthetic primer by the telomerase enzyme leads to non-uniform "elongation products" (telomerase specific 6-nucleotide increments). These are then amplified by Taq DNA Polymerase. The amplification product was denatured and incubated for 10min at room temperature (denaturation reagent, Roche Diagnostics), then hybridized over 2h at 37°C (hybridization buffer, Roche Diagnostics) to digoxigenin-labeled detection

probes. The hybridization mixtures were transferred to streptavidin-coated microplate modules and incubated for another hour at 37°C. The wells were washed (washing solution, Roche Diagnostics) three times before Anti-DIG-POD working solution (containing anti-digoxigenin-peroxidase, Roche Diagnostics) was added. The plate was covered with foil and incubated for 30min at room temperature while shaking at 300rpm. The samples were rinsed 5 times (washing solution, Roche diagnostics) and TMB substrate solution (Roche diagnostics) containing the POD substrate 3,3´,5,5´-tetramethyl benzidine was added. After 20min of color development at room temperature, the stop reagent (Roche diagnostics) was added and the absorbance at 450nm was measured against blank of 750nm using a microplate reader within 20min after addition of the stop reagent. Results are reported as absorbance values: $\Delta A = A_{450} - A_{750}$. Samples are considered positive if the difference in absorbance ΔA is higher than 0.2

3.5 In-situ Q-FISH (quantitative fluorescent in-situ hybridization)

Paraffin sections of cryopreserved tissue-engineered explanted grafts, the anastomosis site and its adjacent vascular tissue, respectively, were dewaxed and rehydrated in descending ethanol series and rinsed with PBS. After incubation in sub-boiling citrate buffer for a cumulative 30 minutes, the slides were incubated for 10min in pepsine solution (1mg/ml ,pH 2.0) at 37°C. After dehydration in ascending ethanol series, the slides were air dried before adding 15µl of the hybridization mix containing 70% formamide, 0.5µg/ml PNA probe (5µl/250µl, 25µg/ml PNA), 0.5% Blocking reagent (12.5µl/250µl,10% Solution, Roche), 8.56% Magnesiumchloride buffer (25mM Magnesiumchloride, 9mM Citric acid, 82mM Disodiumhydrogenphosphate) and 10% 1M Tris pH 7.2. DNA was denatured by heat treatment for 3min at 80°C. After hybridization for 2h in a humid chamber, slides were washed with 70% Formamid/10mM Tris pH 7.2/0.1% BSA followed by TBS-Tween 1% and PBS. Slides were dehydrated using ascending ethanol series and air dried. Antifade and DAPI (Vectashield, Vector #H1200) mounting solution and a coverslip were applied. Digital images were recorded with a Leica microscope equipped with a monochromatic digital

camera (Leica Microsystems, Wetzlar, Germany). Image analysis was performed with TFL-Telo Version 2.2 for Windows software as describe by Poon and Landsorp [55].

Fluorescence intensities of PNA labeled telomeres were measured in the central part of the tissue engineered construct and compared to sections which included native vascular tissue adjacent to the anastomosis site on the same histological section.

3.6 Statistical Analysis

Statistical analysis including histograms and boxplots was carried out with PASW Statistics Version 18 for Windows (SPSS Inc., Chicago, IL, USA). Q-FISH data underwent a Mann-Whitney-U-Test to test for statistical significance. The null-hypothesis was rejected for p-values greater than 0.05.

3.7 Immunohistological Analysis

Immunohistochemistry was performed using the Ventana Benchmark automated staining system (Ventana Medical Systems, Tuczon, Arizona) and the following primary antibodies: Anti-vimentin (clone 3B4, DakoCytomation, Glostrup, Denmark), anti-desmin (clone D33, DakoCytomation, Glostrup, Denmark) and anti-α-smooth muscle actin (α-SMA, clone 1A4, Sigma Chemical Company, St. Louis, MO, USA), anti-vascular endothelial growth factor (VEGF) (AK77, Lab Visison, Fremont, CA, USA) and anti-Ki67 (Mib-1, DakoCytometry). Primary antibodies were detected with the Ventana iVIEW DAB detection kit, resulting in a brown reaction product. Slides were counterstained with haematoxylin and covered with a glass cover slip.

4 Results

4.1 Telomerase Activity (TRAP and ELISA)

Measurement of telomerase activity in three different ovine myofibroblast cell cultures (OVS and OVJ respectively) passaged three to four times (P3 and P4) yielded negative results with a mean absorbance values of five different measurements at 450nm of 0.063 A_{450}-A_{750} for OVS 1 P3, 0.076 A_{450}-A_{750} for OVJ 2 P3 and 0.051 A_{450}-A_{750} OVJ 3 P4 against the reference wavelength of 750nm. Samples are considered negative if the difference of negative controls (not shown in the graph) to the corresponding samples is less than 0.2 A_{450}-A_{750} units. The assay was validated with positive controls supplied by the manufacturer within the specified range (higher than 1.5 A_{450}-A_{750}). We also measured telomerase activity in 1301 cell line, which was later used to determine relative telomere length. It showed active telomerase as expected.

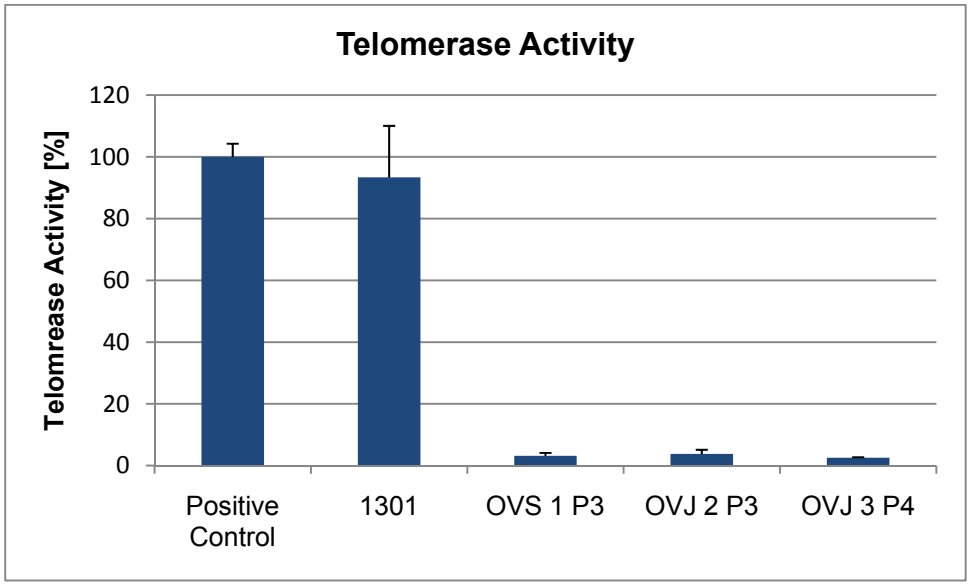

Figure 4: **Telomerase activity of ovine myofibroblasts (OVS 1 P3, OVJ2 P3 and OVJ 3 P4). The absence of telomerase activity in all measured ovine myofibroblasts is confirmed by positive results for the positive contol (supplied by the manufacturer) and the telomerase-active 1301 cell line. The error bars indicate +1 Standard Deviation over all measurements.**

4.2 Flow- FISH / Telomere length

Relative Telomere length (RTL) of three Swiss Alpine lambs were measured after 2-4, 13-16, 26-32 and 44-54 population doublings. Cells of all lambs were measured in two separate experiments as shown in Figure 5 to ensure internal consistency of the obtained results. Serial passaging of myofibroblasts with a mean population doubling time of approximately 31-38 hours for all ovine myofibroblasts resulted in a decrease of relative telomere length of 25.8%-32.3% over 41-44 population doublings with an approximate linear reduction of relative telomere length as indicated by the coefficients of determination tending towards 1.0 ($R^2_{OVS\ 1A}$=0.9981, $R^2_{OVS\ 2A}$=0.9365 and $R^2_{OVJ\ 3A}$=0.988) for linear regression. One sheep (OVS 1) showed significantly longer RTL than the other two, pointing towards interindividual differences of absolute telomere length [56]. However, Flow-FISH was not sensitive enough to reliably separate mixed cell populations with different population doublings.

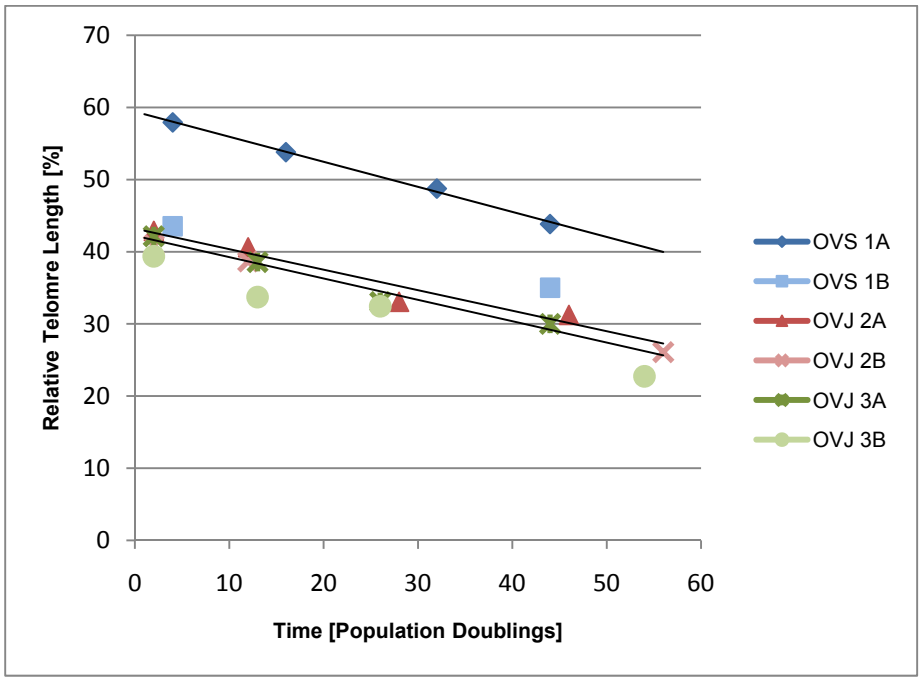

Figure 5: Overview of all measured relative telomere lengths. RTL of the saphenous vein (OVS 1) were significantly higher than in the other two lambs (OVJ 2 and 3). This may be due to interindivdual differences or the different isolation location (saphenous vs. external jugular vein in OVJ 2 and 3)

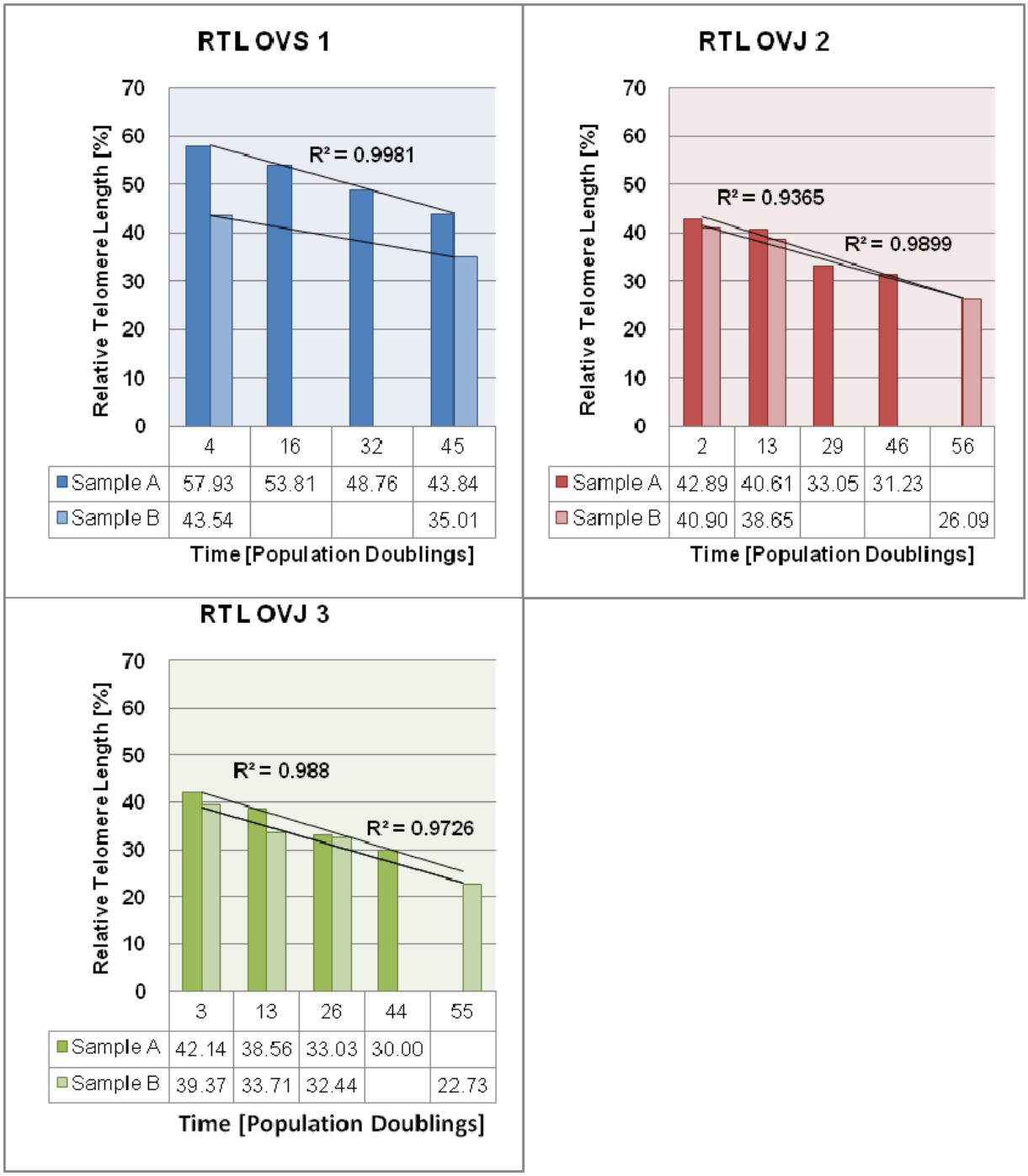

Figure 6: **Decrease of Relative Telomere Lengths of isolated ovine myofibroblasts. All measured cell lines showed an approximate linear decrease of telomere lengths. Each cell line was measured in two individually processed samples (Samples A and B).**

4.3 Telomere Fluorescence in TEVG vs. Native

After follow-up periods of 5, 20, 50, 100 and 240 weeks, tissue-engineered pulmonary artery conduits and native vessel wall neighboring the anastomosis site from 5 Swiss Alpine Lambs were explanted, fixed and embedded in paraffin wax until further use. Sections were made from each of the three regions of interest, the central part of the conduit (TEVG), the anastomosis site and native vessel (Native), respectively. 1-3 sections of the central part of the conduit and the native vessel were processed and images captured of 10 different regions on the slides. Slides were processed for Telomere Q-FISH analysis. For each slide region the median fluorescence value was computed, accounting for data outliers caused by bad image quality or staining errors.

4.3.1 5 Weeks TEVG vs. Native

5 weeks post implantation specimens of TEVG and Native showed equally distributed fluorescence intensities across all measured datasets. 29 datasets for Native and 30 datasets for TEVG recorded from three different slides were available for analysis. Results show a lower mean and median value for TEVG compared to Native. A conducted Mann-Whitney-U-Test attested statistical significance for the obtained distribution with a p-value <0.01. As a consequence, telomere lengths of the TEVG are significantly shorter than those of its native counterpart.

5 Weeks		Statistic	Std. Error
TEVG	Mean	1386.03	22.462
	Median	1004.24	
	Variance	1260317.857	
	Std. Deviation	1122.639	
Native	Mean	2149.19	32.635
	Median	1211.70	
	Variance	6264476.805	
	Std. Deviation	2502.894	

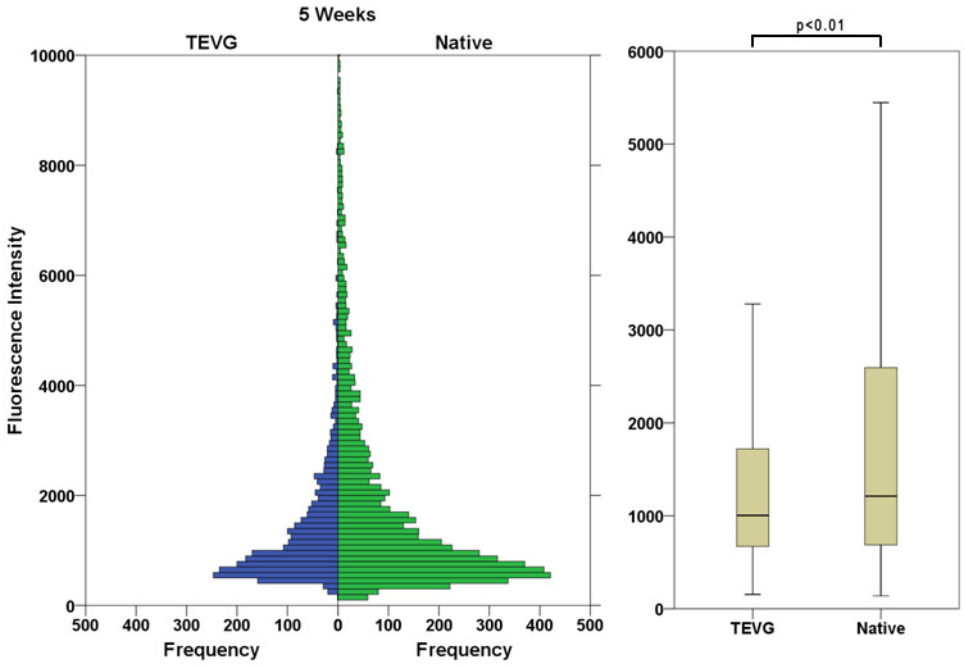

Figure 7: Histogramm of measured fluorescence intensities 5 weeks post implantation. The boxplot shows minimum, first quartile, median, third quartile, and maximum. Extreme values are not shown in the plot. The Mann-Whitney-U-Test shows statistical significance for distribution with p<0.01.

4.3.2 20 Weeks TEVG vs. Native

20 weeks post implantation, 2 sets of slides of two different sheep were available for analysis. The first Set (Set 1) contained 29 datasets for Native and 30 datasets for TEVG recorded from three slides each. The second Set (Set 2) contained 18 datasets for Native and 20 datasets for TEVG recorded from 3 and 2 slides, respectively. S1 distribution descriptively shows a different mean (1676.61 vs. 2102.17) value with only slightly differing medians (1090.06 vs. 1133.24). In contrast to S2, a Mann-Whitney-U-Test on S1 failed to show a statistically significant difference in distribution (p=0.155).

20 Weeks Set 1		Statistic	Std. Error
TEVG	Mean	1676.61	37.288
	Median	1090.08	
	Variance	2690386.424	
	Std. Deviation	1640.240	
Native	Mean	2102.17	36.680
	Median	1133.24	
	Variance	6646471.432	
	Std. Deviation	2578.075	

20 Weeks Set 2		Statistic	Std. Error
TEVG	Mean	1595.91	39.548
	Median	954.58	
	Variance	2984178.391	
	Std. Deviation	1727.477	
Native	Mean	2996.74	65.548
	Median	1622.14	
	Variance	1.156E7	
	Std. Deviation	3400.315	

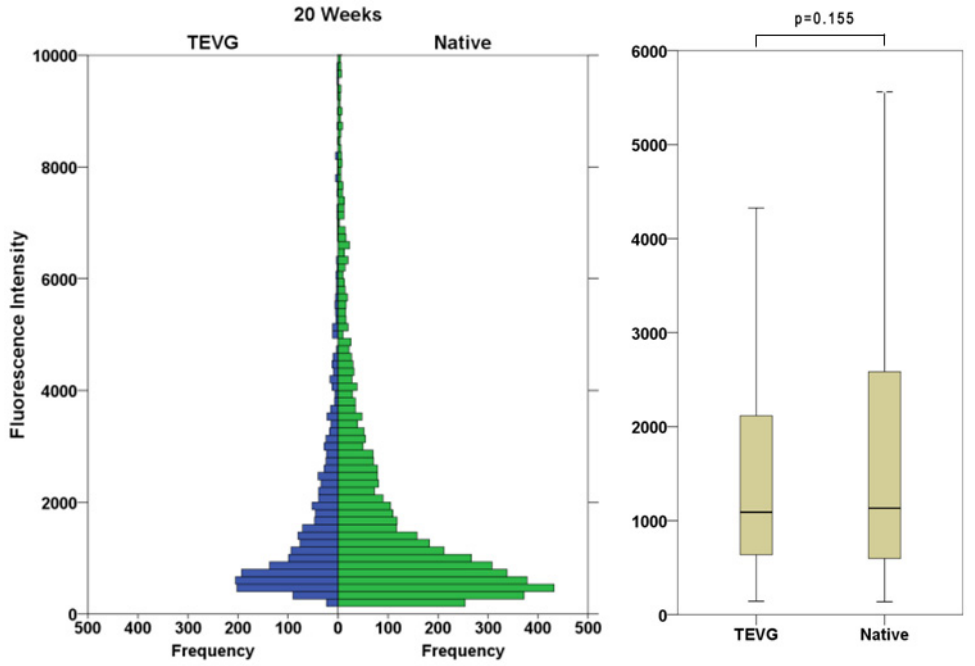

Figure 8: Histogramm of measured fluorescence Intensities 20 weeks post implantation (Set 1). The boxplot shows minimum, first quartile, median, third quartile, and maximum. The Mann-Whitney-U-Test shows no statistically significant difference in distribution.

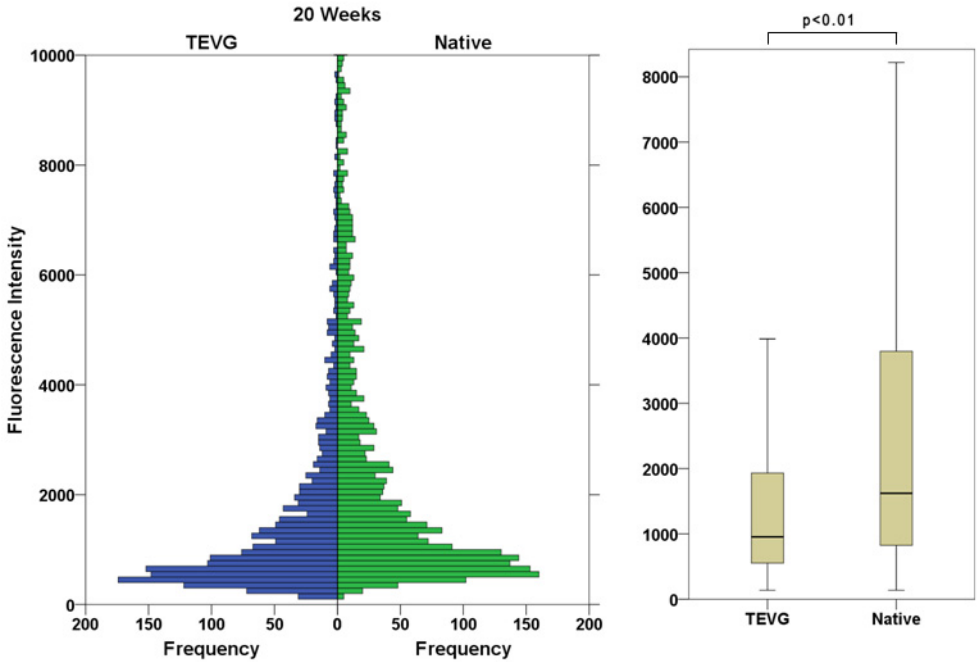

Figure 9: Histogramm of measured fluorescence Intensities 20 weeks post implantation (Set 2). The boxplot shows minimum, first quartile, median, third quartile, and maximum. The Mann-Whitney-U-Test shows statistical significance in distribution with $p<0.01$.

4.3.3 50 Weeks TEVG vs. Native

50 weeks post implantation, 7 datasets for Native and 18 datasets for TEVG were available for analysis. Results show a statistically significant lower median value for TEVG (1065.71) vs. Native (1601.38) with $p<0.01$.

50 Weeks		Statistic	Std. Error
TEVG	Mean	1698.13	40.176
	Median	1065.71	
	Variance	3147488.965	
	Std. Deviation	1774.116	
Native	Mean	2876.54	104.724
	Median	1601.38	
	Variance	1.016E7	
	Std. Deviation	3186.784	

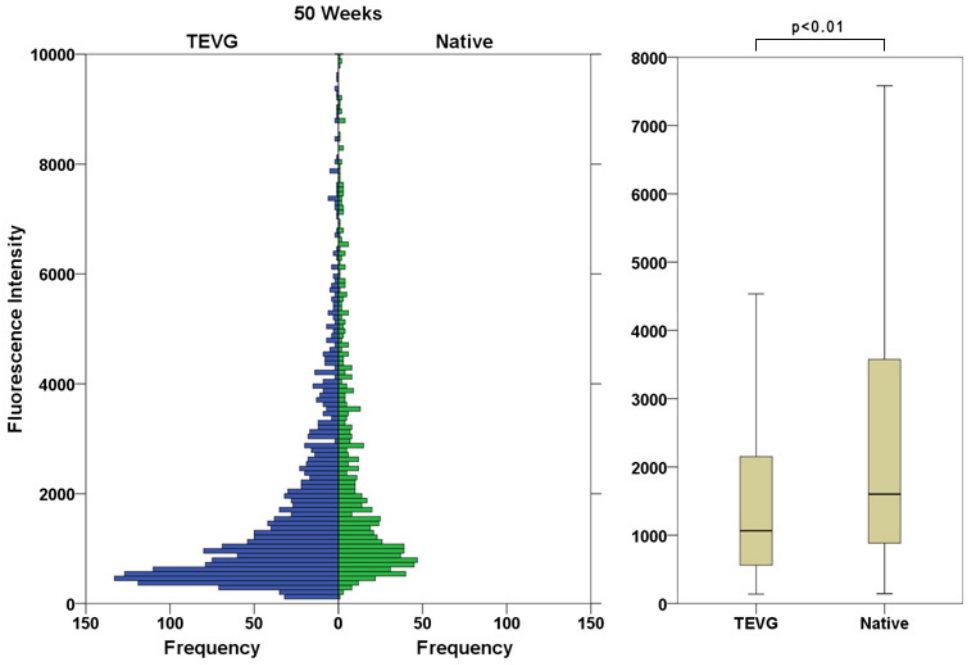

Figure 10: **Histogram and Boxplot 50 weeks post implanation. For Native n=936 datapoints were included. The Mann-Whitney-U-Test shows statistical significance in distribution with p<0.01.**

4.3.4 100 Weeks TEVG vs. Native

100 weeks post implantation, 2 sets of slides from two different sheep were available for analysis. The first Set (S1) contained 25 datasets for Native and TEVG each. The second Set (S2) contained 28 datasets for Native and 29 datasets for TEVG. For both Sets, the median values of the TEVG (1068.02 and 856.87) were significantly lower than those of Native (1601.38 and 1114.05) with p<0.01 for both sets.

100 Weeks Set 1		Statistic	Std. Error
TEVG	Mean	1245.78	20.766
	Median	856.87	
	Variance	1575268.451	
	Std. Deviation	1255.097	
Native	Mean	1967.64	32.784
	Median	1114.05	
	Variance	5647060.934	
	Std. Deviation	2376.355	

100 Weeks Set 2		Statistic	Std. Error
TEVG	Mean	1854.67	47.108
	Median	1068.02	
	Variance	4751187.234	
	Std. Deviation	2179.722	
Native	Mean	2020.33	36.484
	Median	1250.12	
	Variance	4549733.711	
	Std. Deviation	2133.010	

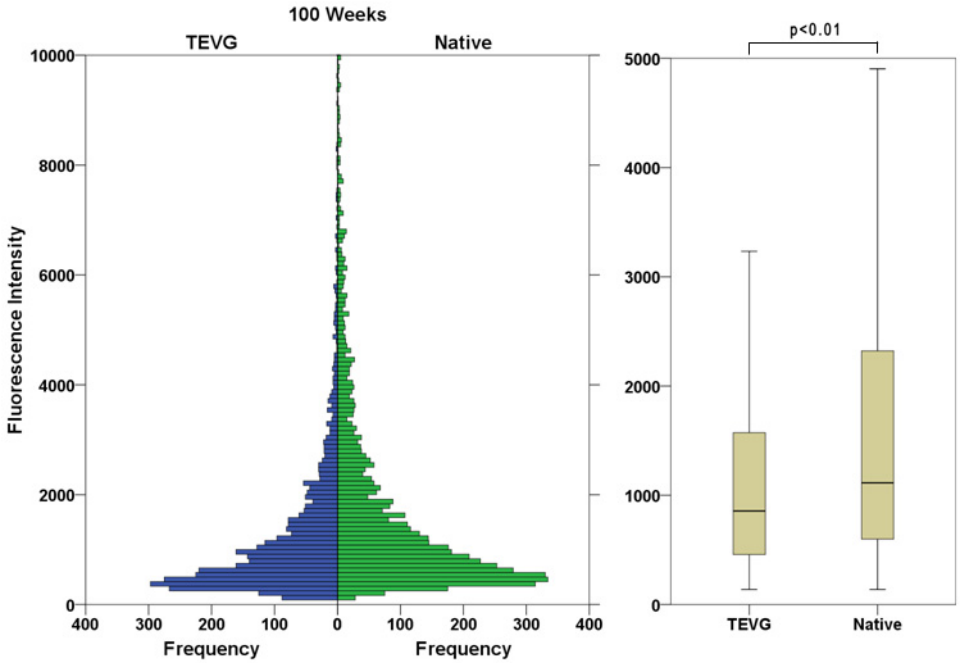

Figure 11: Histogramm of measured fluorescence Intensities 100 weeks post implantation (Set 1). The boxplot shows minimum, first quartile, median, third quartile, and maximum. The Mann-Whitney-U-Test shows statistical significance in distribution with a p<0.01.

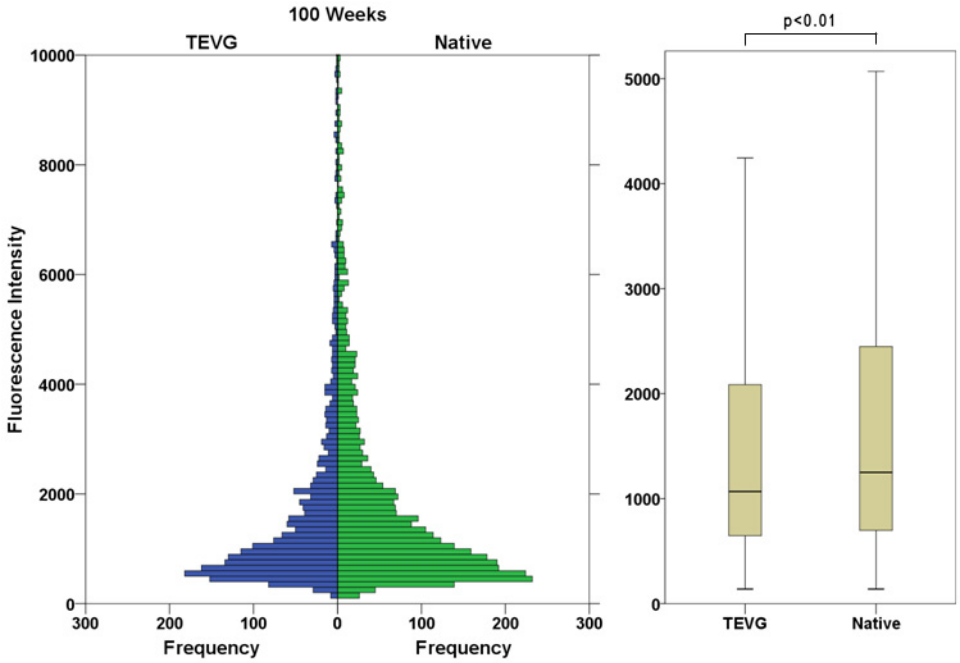

Figure 12: Histogramm of measured fluorescence Intensities 100 weeks post implantation (Set 2). The boxplot shows minimum, first quartile, median, third quartile, and maximum. The Mann-Whitney-U-Test shows statistical significance in distribution with a $p<0.01$.

4.3.5 240 Weeks TEVG vs. Native

240 weeks post implantation specimens of TEVG and Native showed unevenly distributed fluorescence intensities across the measured datasets. 25 datasets for Native and 17 datasets for TEVG were available for analysis. After correcting for data outliers, a statistical significance between Native and TEVG telomere length could not be detected. However, compared to the other measured datasets, this set contained large differences in the means of each slide, especially in the TEVG, where median fluorescence values range from 327 arbitrary units to 1230.22 units in the acquired datasets. Details are shown in Figure 14. This implies that some cells have very short telomeres, whereas a considerable amount of cells has telomere lengths comparable to the native vessel (range 453.16 to 1016.9 arbitrary units).

240 Weeks		Statistic	Std. Error
TEVG	Mean	1012.68	42.425
	Median	664.12	
	Variance	1078111.907	
	Std. Deviation	1038.322	
Native	Mean	1033.42	27.732
	Median	660.46	
	Variance	1245867.486	
	Std. Deviation	1116.184	

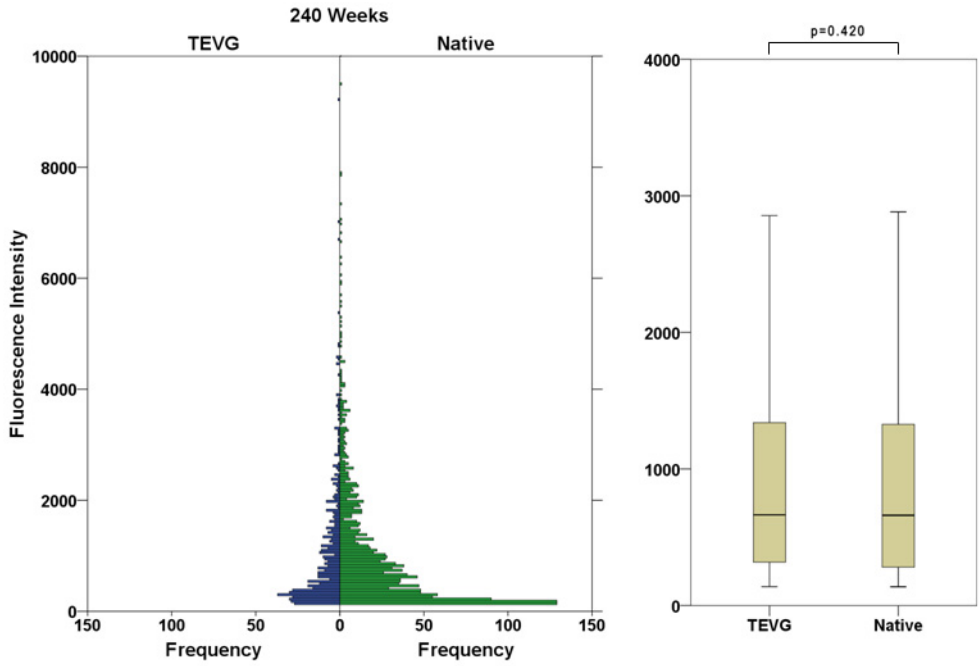

Figure 13: **Histogramm of measured fluorescence Intensities 240 weeks post implantation. The boxplot shows minimum, first quartile, median, third quartile, and maximum. A statistically significant difference in distribution could not be detected.**

4.3.6 Overview of mean and median fluorescence intensities of acquired datasets

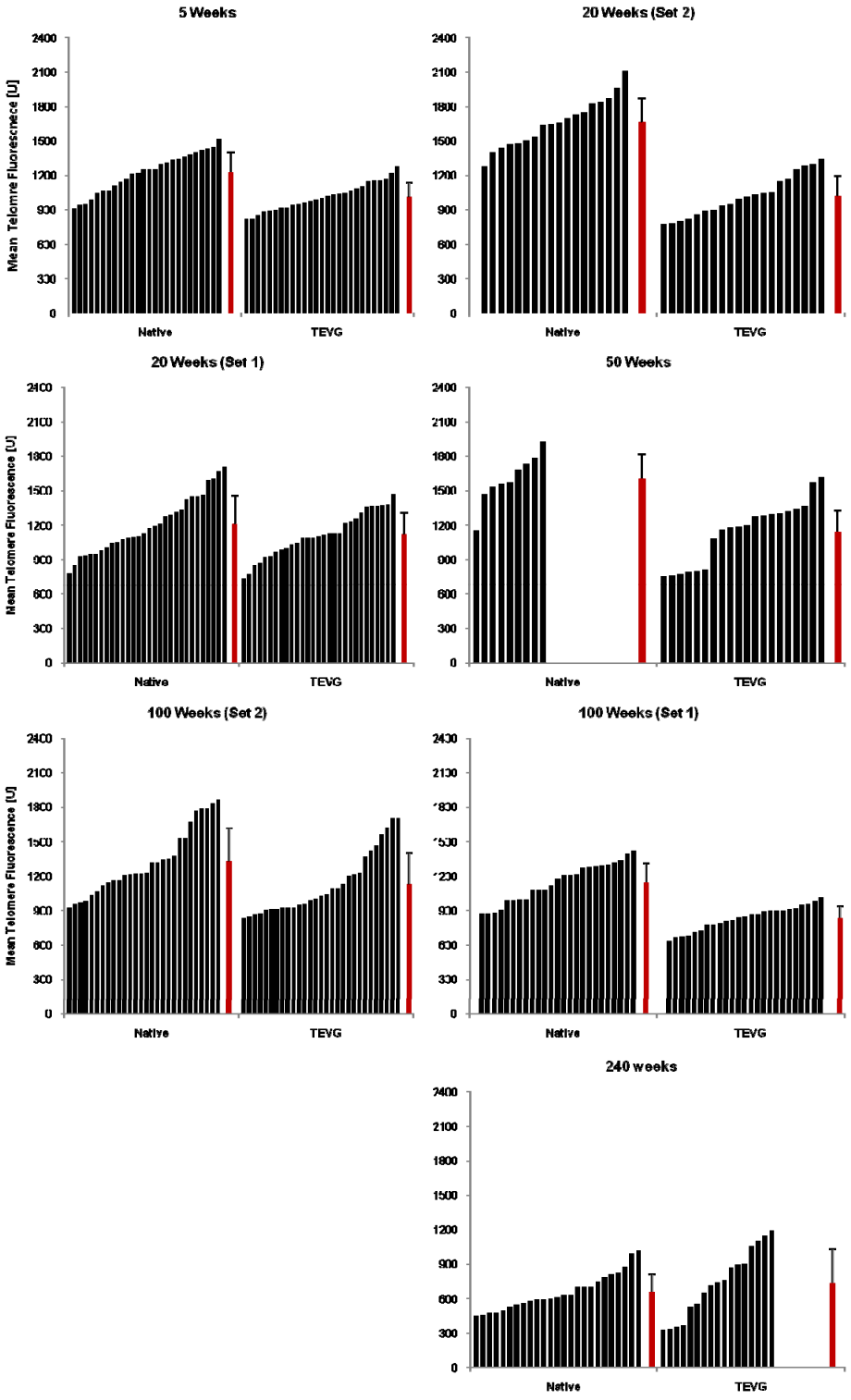

Figure 14: Measured median fluorescence values of the telomeric probes and calculated median of all explanted TEVG and Native tissue. The black bars represent the median values of measured fluorescent intensites of the individual slides. The red bars represent the mean of all measured medians. The error bars represent 1 standard deviation over all measurements.

4.4 Histological Analysis of Tissue Remodeling

Histological analyses from sections of tissue engineered pulmonary arteries obtained after 20 and 100 weeks post implantation and native tissue histologically show similarly configured TEVGs (A and F) compared to Native (K) with an endothelial layer to the luminal side with scattered smooth muscle cells and proprietary capillary vessels embedded in a fibrous tissue in the tunica media and its adjacent adventitia. Staining for the proliferation marker Ki67 [57] shows increased proliferative activity within the TEVGs (B and G) in the media. Likewise, VEGF could be identified in the TEVGs (C and H), but mainly co-localized around residual fibers within polynucleated giant cells, therefore arguing against a state of ubiquitous hypoxia in TEVG. At the anastomosis site, a growth cone positive for Desmin, an intermediate filament in the cytoskeleton of smooth muscle cells [58], is visible after 20 and 100 weeks (D and I), suggesting a continuous merging and replacement of cells with a smooth muscle phenotype into the tissue-engineered graft. The latter are characterized by positive staining for Desmin and alpha-SMA [59]. (N) illustrates the localization of the histological specimens from the center of the graft as well as from the anastomosis.

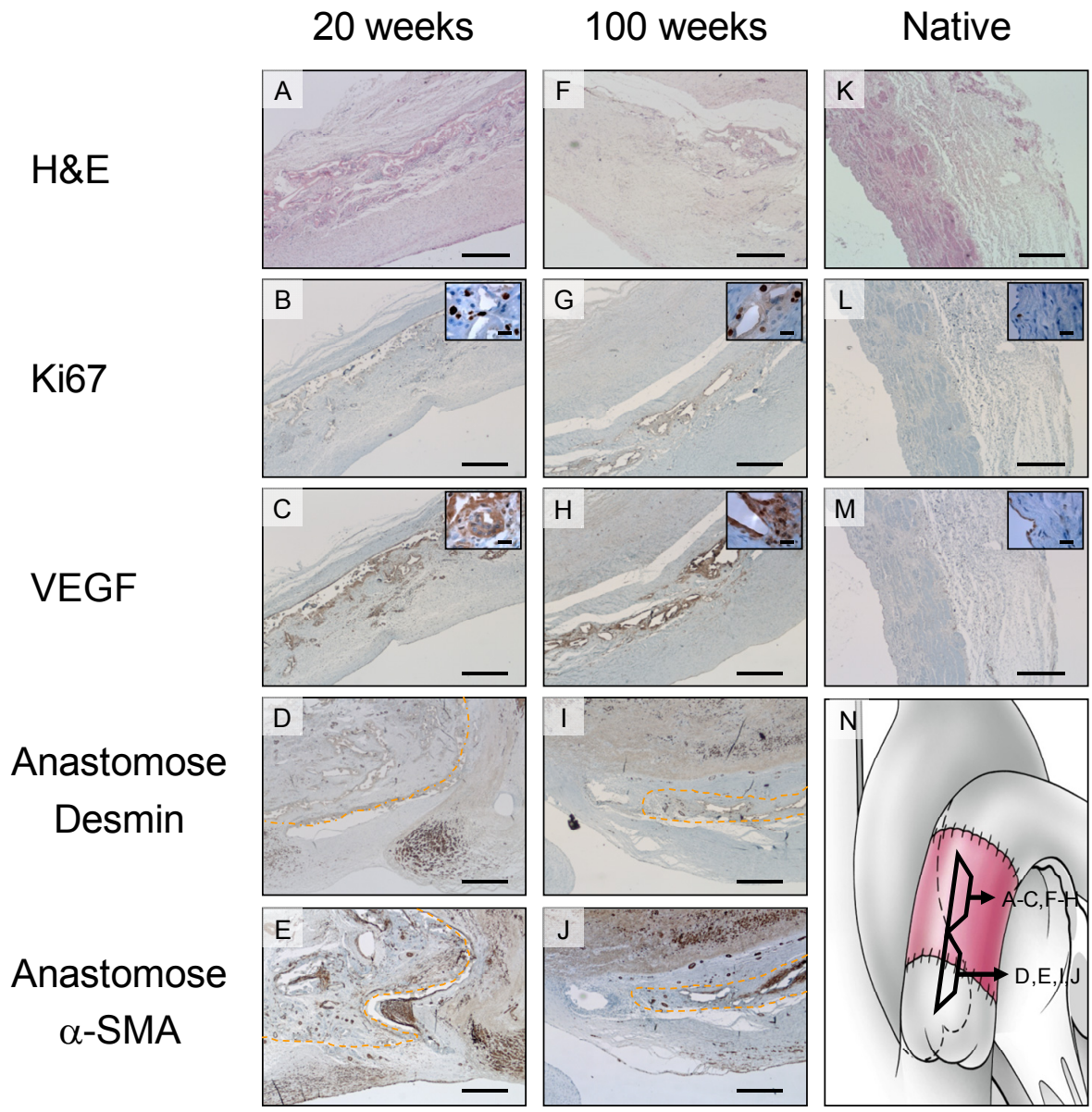

Figure 15: Overview of immunohistological analyses 20 and 100 weeks post implantation.

5 Discussion

5.1 Telomere Flow-FISH and Q-FISH analysis

Flow-FISH provides an interesting tool to evaluate large cell numbers and is especially useful when cells are in a suspended state, typically during the fabrication process of TEVG. We used a commercially available kit to assess telomere lengths during the expansion of ovine myofibroblasts. The results show an approximately linear reduction of relative telomere length during serial passaging. As a consequence, telomere lengths differ only slightly in the lower range between 2 and 16 population doublings, which is normally the desired range for tissue engineering purposes. Telomerase was shown to be absent in all measured cell populations and therefore has no implication in this experimental setting. Yet, mixed cell populations with large differences in population doublings could not be distinguished by Flow-FISH because of the wide range of the measured fluorescence values corresponding to telomere length (see appendix for details). This poses the main drawback to distinguish native cells and cells originating from tissue engineered constructs using telomere length determination by Flow-FISH.

In-situ based Q-FISH determines telomere length on a single cell basis staining for telomeric sequences with peptide nucleic acid (PNA) of all exposed chromosomes. Quantification can be obtained by using internal controls and fluorescent beads to correct for differences in staining intensities, exposure times and fluorescence lamp intensity variations [60]. Our results clearly indicate that telomeres are shorter in almost all measured samples of TEVG compared to the native vessel. How this is thought to be related to cellular aging, graft fabrication and remodeling processes is discussed in the following sections. Different median fluorescent intensities of all measured Native samples between different sheep may be due to differences in sample quality and processing or due to inter-individual differences of the lambs. As described above, quantitative analysis would require the additional use of fluorescent beads and internal controls with cells with already known telomere length, which

are commercially available. This should be included in future studies. Furthermore, telomere length measurements using in-situ based Q-FISH before and after the bioreactor phase would allow for quantification of telomere length reduction during the individual fabrication processes and could even be quantified in relation to post-implantation processes.

5.2 Remodeling processes

Understanding the cellular remodeling processes after graft implantation is crucial to facilitate the design of tissue replacements in regard to functionalized scaffold materials [61] and suitable cell sources [6, 62]. According to the presented results, there is strong evidence by histological, phenotypical and cell ageing analyses that in a growing organism, the myofibroblasts used to produce the TEVG are being at least partially replaced by native cells surrounding the TEVG. Several mechanisms are feasible by which the cells are replaced: (i) classical inflammation and connective tissue repair by the recipient which then remodels to functional tissue with near-appropriate cell phenotypes and extracellular matrix [63]; (ii) homing of blood-bound stem or progenitor cells that settle within the graft; (iii) myofibroblasts invade the TEVG from the adventitia surrounding the graft; (iv) the TE graft is invaded/encapsulated from the sides of the anastomosis and (v) a combinatorial mechanism from the above mentioned. The proposed mechanisms are illustrated in Figure 16.

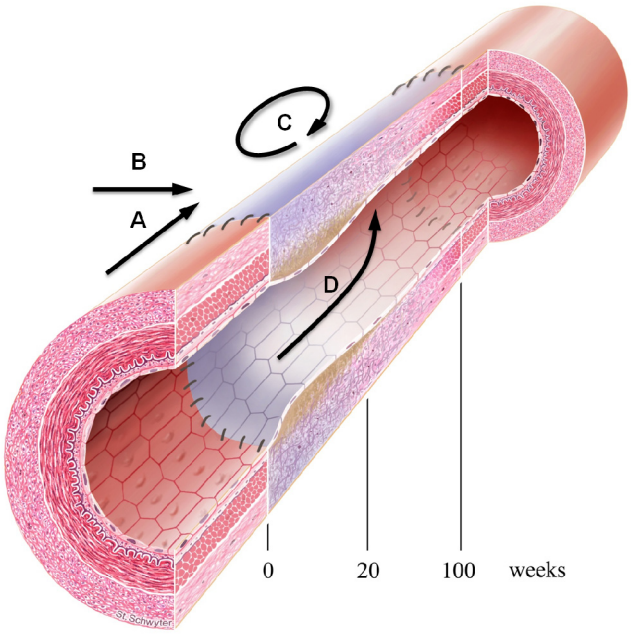

Figure 16: **Remodelling processes over 100 weeks of a tissue engineered vascular graft. [A:] Ingrowth from the sides of anastomosis and the adjacent adventitia [B]. [C] represents in-graft remodeling via inflammation and growth processes. [D]: Recruitment of circulating stem or progenitor cells. Time indicators show the progression of remodeling processes towards a fully functional graft resembling native vascular tissue over a completed growth cycle of the animal model.**

5.3 Scaffold material

Based on the proposed remodeling processes, our observations indicate that grafts for cardiovascular tissue engineering need to serve as synthetic or living biological matrix that guides and/or induces healing processes in vivo, which clearly is mediated by endogenous cells.

In vascular tissue engineering, the scaffold typically is a resorbable polymer with key biological information that drives effective functional remodeling of the substrate. Off-the-shelve grafts would be superior to “functionalize” fast degrading polymers with autologous cells in biomimetic reactors. Yet, this is a complex and time consuming process. The demands on such biomaterials are very high: (i) adequate mechanical strength but still elastic to propagate the sinus wave, (ii) immunological inert, (iii) no tendency to stenosis or

stricture formation, (iv) enable controlled cellular ingrowth, (v) well balanced scaffold degradation - tissue formation kinetic and (vi) not subject to immediate or fast calcification.

To match the complexity of mechanical, cellular and molecular biological cues provided by living engineered tissues, will be a highly challenging attempt to be recreated by biomaterial scientists. First steps towards functionalized tissues have been taken. Carbon nanotubes may aid in the process of tissue development not only as a structural reinforcement of today's typically used scaffolds in the fabrication process [64,65] but also as a part of a functionalized scaffold material with directed cell growth for example by using the electrical conductivity of carbon nanotubes [22,66]. Furthermore, they can potentially be used to release bioactive factors to provide a scaffold material tailored to demand.

5.4 Aging of TEVG

The obtained results show that telomere length in tissue-engineered grafts is, for the most part, significantly lower than in the native arteries. There are several mechanisms possible as how telomere length can be decreased: (i) An increased cell turnover during the remodeling process due to increased shear stress and inflammation processes. This was also proposed by Okuda et al. [67], who detected shorter telomeres in parts of the aortic wall with a higher shear stress, a factor, which could also play a role in this animal model before, during the bioreactor phase, or after implantation. Matthews et al. [68] detected a decrease in telomere length with a quantitative telomere/immunostaining fluorescence in-situ hybridization (TELI-FISH) in atherosclerotic plaques in human vascular smooth muscle cells (VSMC) compared to cells in the tunica media of the same lesion. This was thought to be due to additional replications involved in lesion development but he also identified (ii) oxidative stress to have a substantial influence on telomere length in vitro. Similar results came from Kurz et al. [69]. Even though we could not detect an ubiquitous appearance of VEGF in the graft by immunohistochemistry, a higher oxidative stress in the grafts due to insufficient proprietary small vessels during the first phase after implantation cannot be ruled out. Based on the demonstrated remodeling processes, we have to conclude that telomeres are reduced at

least partly due to cell division or replacement. Even though our data show, that telomeres are reduced during the initial fabrication process, some grafts show no significant difference in telomere length, suggesting that the observed decreased telomere length in the TEVG is not solely explained by cell expansion during the fabrication process. Also, the time necessary to reach a sufficient number of cells typically does not exceed a 14 day period, which corresponds to approximately 10 populations doublings (calculated by a mean population doubling speed of 35 hours) in this animal model. Our data suggest that telomere length is not substantially decreased during this time period. Unfortunately, the lack of pre-implant telomere analysis does not allow us to quantify which process (expansion and bioreactor phase or post-implantation processes) affects telomere lengths the most.

5.5 Clinical implications

Tissue engineering, and in this particular case TEVG positioned in a pulmonary artery, aims at eventually providing an alternative approach to the reparation of congenital cardiac lesions. Current conduits for reconstruction of the right ventricular outflow tract (RVOT) consist of valved aortic or pulmonary homografts or stented bovine or porcine xenografts and other prosthetic conduits [70], whereas the pulmonary homograft is considered the gold standard. Major drawbacks, in many cases, include the need of graft replacement due to conduit failure during growth and development of the patients. A failure rate of approximately 40% at 10 years has been reported [71]. Conduit failure is not limited to somatic outgrowth and includes conduit contracture or shrinkage, conduit kinking, sternal compression, posterior muscle shelf impingement and distal anastomotic stenosis [71]. Also, immunologic reactions to the implanted homografts are held responsible for conduit failure as proposed by Neves et al. [72] and Hawkins et al. [73] amongst others.

Thus far, autologous cell-based tissue-engineered vascular grafts have been shown to be largely free of side effects such as dilatation, stenosis, acute and chronic inflammatory responses or thrombus formation [6]. We have shown that production and remodeling processes of TEVG lead to a premature aging, expressed in shorter telomere lengths.

Further analyses by Hoerstrup and coworkes show that the implanted TEVG are fully functional over a complete lifecycle of the chosen animal model. This implies that telomeres overall do not shorten to a critical length, which may lead to cellular senescence. As we have seen from the results 240 weeks post implantation, telomere lengths of the TEVG were highly variable. This could be due to ongoing remodeling or inflammation processes coupled with extensive cellular replacement, and thus restoring mean telomere length and replacing dysfunctional and maybe senescent cells. From a clinical point of view and accounting for the results obtained in this study, conduit replacements during a patient's lifetime may not be completely avoided. Yet, it is possible that necessary re-operations may be deferred to a more convenient point of time. Most importantly, results have showed that the implanted grafts survive in a fully functional state and grow over the host animal's life cycle.

However, the dogma of tissue engineers to create fully functional biological substitutes to enable adequate immediate and long-term *in vivo* functionality has to be questioned. Implantation of TE grafts which are developed to a point at which they have developed enough extracellular matrix to cope with the mechanical demands might be sufficient for long-term in vivo functionality. To further unravel the complex mechanisms of cellular remodeling and replacement processes of tissue engineered grafts, future efforts of biomaterial scientists and tissue engineers will be mandatory to optimize the design parameters of cardiovascular grafts and their successful clinical use in the future.

Telomeres are currently highly focused on in the field of aging and development, as well as experimental oncology to develop new methods for tumor suppression. Tissue engineering is represented in all these domains, trying to offer new treatment strategies and concepts. With further advances in the field of tissue engineering in regard to the development of biomaterials and cell sources, the demand for monitoring methods is continuously rising. We conclude that through this study, we have successfully added telomere length analysis to this toolbox.

6 References

1. Hoerstrup, S.P., et al., *Tissue engineering of small caliber vascular grafts.* Eur J Cardiothorac Surg, 2001. **20**(1): p. 164-9.
2. Hoerstrup, S.P., et al., *Functional living trileaflet heart valves grown in vitro.* Circulation, 2000. **102**(19 Suppl 3): p. III44-9.
3. Lunde, K., et al., *Intracoronary Injection of Mononuclear Bone Marrow Cells in Acute Myocardial Infarction.* N Engl J Med, 2006. **355**(12): p. 1199-1209.
4. Strauer, B.E., et al., *Repair of Infarcted Myocardium by Autologous Intracoronary Mononuclear Bone Marrow Cell Transplantation in Humans.* Circulation, 2002. **106**(15): p. 1913-1918.
5. Langer, R. and J.P. Vacanti, *Tissue engineering.* Science, 1993. **260**(5110): p. 920-6.
6. Hoerstrup, S.P., et al., *Functional growth in tissue-engineered living, vascular grafts: follow-up at 100 weeks in a large animal model.* Circulation, 2006. **114**(1 Suppl): p. I159-66.
7. Stock, U.A., et al., *Patch augmentation of the pulmonary artery with bioabsorbable polymers and autologous cell seeding.* J Thorac Cardiovasc Surg, 2000. **120**(6): p. 1158-1167.
8. Matsumura, G., et al., *First Evidence That Bone Marrow Cells Contribute to the Construction of Tissue-Engineered Vascular Autografts In Vivo.* Circulation, 2003. **108**(14): p. 1729-1734.
9. Mettler, B.A., et al., *Stem Cell-Derived, Tissue-Engineered Pulmonary Artery Augmentation Patches In Vivo.* The Annals of Thoracic Surgery, 2008. **86**(1): p. 132-141.
10. Sales, V.L., et al., *Endothelial Progenitor and Mesenchymal Stem Cell–Derived Cells Persist in Tissue-Engineered Patch In Vivo: Application of Green and Red Fluorescent Protein–Expressing Retroviral Vector.* Tissue Engineering, 2007. **13**(3): p. 525-535.
11. Mendelson, K., et al., *Healing and remodeling of bioengineered pulmonary artery patches implanted in sheep.* Cardiovascular Pathology, 2007. **16**(5): p. 277-282.
12. Shinoka, T., et al., *Creation Of Viable Pulmonary Artery Autografts Through Tissue Engineering.* J Thorac Cardiovasc Surg, 1998. **115**(3): p. 536-546.
13. Lisa, K., et al., *Feridex labeling of mesenchymal stem cells inhibits chondrogenesis but not adipogenesis or osteogenesis.* NMR in Biomedicine, 2004. **17**(7): p. 513-517.
14. Parish, C.R., *Fluorescent dyes for lymphocyte migration and proliferation studies.* Immunol Cell Biol, 1999. **77**(6): p. 499-508.
15. Yanagawa, M.C., *FTY720, a novel immunosuppressant, induces sequestration of circulating mature lymphocytes by acceleration of lymphocyte homing in rats, III. Increase in frequency of CD62L-positive T cells in Peyer's patches by FTY720-induced lymphocyte homing.* Immunology, 1998. **95**(4): p. 591-594.
16. Weston, S.A. and C.R. Parish, *New fluorescent dyes for lymphocyte migration studies: Analysis by flow cytometry and fluorescence microscopy.* Journal of Immunological Methods, 1990. **133**(1): p. 87-97.
17. Rivella, S. and M. Sadelain, *Genetic treatment of severe hemoglobinopathies: the combat against transgene variegation and transgene silencing.* Semin Hematol, 1998. **35**(2): p. 112-25.
18. Strable, E., et al., *Synthesis and Characterization of Soluble Iron Oxide−Dendrimer Composites.* Chemistry of Materials, 2001. **13**(6): p. 2201-2209.
19. Glenn A. Walter, K.S.C.J.H.H.F.T.D.H.L.S.J.W.M.B., *Noninvasive monitoring of stem cell transfer for muscle disorders.* Magnetic Resonance in Medicine, 2004. **51**(2): p. 273-277.

20. Terrovitis, J., et al., *Magnetic resonance imaging overestimates ferumoxide-labeled stem cell survival after transplantation in the heart.* Circulation, 2008. **117**(12): p. 1555-62.
21. Iijima, S., *Helical microtubules of graphitic carbon.* Nature, 1991. **354**(6348): p. 56-58.
22. Harrison, B.S. and A. Atala, *Carbon nanotube applications for tissue engineering.* Biomaterials, 2007. **28**(2): p. 344-53.
23. Heller, D.A., et al., *Single-Walled Carbon Nanotube Spectroscopy in Live Cells: Towards Long-Term Labels and Optical Sensors.* Advanced Materials, 2005. **17**(23): p. 2793-2799.
24. Sitharaman, B., et al., *Superparamagnetic gadonanotubes are high-performance MRI contrast agents.* Chem Commun (Camb), 2005(31): p. 3915-7.
25. Jaiswal, J.K., et al., *Long-term multiple color imaging of live cells using quantum dot bioconjugates.* Nat Biotech, 2003. **21**(1): p. 47-51.
26. Ghasemi, Y., P. Peymani, and S. Afifi, *Quantum dot: magic nanoparticle for imaging, detection and targeting.* Acta Biomed, 2009. **80**(2): p. 156-65.
27. Muller, P., et al., *Cardiomyocytes of noncardiac origin in myocardial biopsies of human transplanted hearts.* Circulation, 2002. **106**(1): p. 31-5.
28. Albera, C., et al., *Repopulation of human pulmonary epithelium by bone marrow cells: a potential means to promote repair.* Tissue Eng, 2005. **11**(7-8): p. 1115-21.
29. Olovnikov, A.M., *A theory of marginotomy. The incomplete copying of template margin in enzymic synthesis of polynucleotides and biological significance of the phenomenon.* J Theor Biol, 1973. **41**(1): p. 181-90.
30. Blackburn, E.H., *The molecular structure of centromeres and telomeres.* Annu Rev Biochem, 1984. **53**: p. 163-94.
31. Moyzis, R.K., et al., *A highly conserved repetitive DNA sequence, (TTAGGG)n, present at the telomeres of human chromosomes.* Proc Natl Acad Sci U S A, 1988. **85**(18): p. 6622-6.
32. de Lange, T., *T-loops and the origin of telomeres.* Nat Rev Mol Cell Biol, 2004. **5**(4): p. 323-329.
33. Griffith, J.D., et al., *Mammalian telomeres end in a large duplex loop.* Cell, 1999. **97**(4): p. 503-14.
34. Harley, C.B., A.B. Futcher, and C.W. Greider, *Telomeres shorten during ageing of human fibroblasts.* Nature, 1990. **345**(6274): p. 458-60.
35. Chang, E. and C.B. Harley, *Telomere length and replicative aging in human vascular tissues.* Proc Natl Acad Sci U S A, 1995. **92**(24): p. 11190-4.
36. Alexander, B., et al., *Telomere length status of somatic cell sheep clones and their offspring.* Mol Reprod Dev, 2007. **74**(12): p. 1525-37.
37. Allsopp, R.C., et al., *Telomere Shortening Is Associated with Cell Division in Vitro and in Vivo.* Experimental Cell Research, 1995. **220**(1): p. 194-200.
38. Baird, D.M., et al., *Telomere instability in the male germline.* Hum. Mol. Genet., 2006. **15**(1): p. 45-51.
39. Jesper Graakjaer, L.P.H.D.-S.G.T.S.K.K.C.J.-A.L.-V., *The relative lengths of individual telomeres are defined in the zygote and strictly maintained during life.* Aging Cell, 2004. **3**(3): p. 97-102.
40. Hayflick, L., *The Limited in Vitro Lifetime of Human Diploid Cell Strains.* Exp Cell Res, 1965. **37**: p. 614-36.
41. Goldstein, S., *Replicative senescence: the human fibroblast comes of age.* Science, 1990. **249**(4973): p. 1129-33.
42. Wright, W.E., O.M. Pereira-Smith, and J.W. Shay, *Reversible cellular senescence: implications for immortalization of normal human diploid fibroblasts.* Mol Cell Biol, 1989. **9**(7): p. 3088-92.
43. Allsopp, R.C. and C.B. Harley, *Evidence for a Critical Telomere Length in Senescent Human Fibroblasts.* Experimental Cell Research, 1995. **219**(1): p. 130-136.

44. Choudhury, A.R., et al., *Cdkn1a deletion improves stem cell function and lifespan of mice with dysfunctional telomeres without accelerating cancer formation.* Nat Genet, 2007. **39**(1): p. 99-105.
45. Shay, J.W., M.D. West, and W.E. Wright, *Re-expression of senescent markers in deinduced reversibly immortalized cells.* Experimental Gerontology. **27**(5-6): p. 477-492.
46. Harley, C.B., *Telomerase is not an oncogene.* Oncogene, 2002. **21**(4): p. 494-502.
47. Greider, C.W. and E.H. Blackburn, *Identification of a specific telomere terminal transferase activity in Tetrahymena extracts.* Cell, 1985. **43**(2 Pt 1): p. 405-13.
48. Rubin, H., *Cell aging in vivo and in vitro.* Mechanisms of Ageing and Development, 1997. **98**(1): p. 1-35.
49. Amit, M., et al., *Clonally derived human embryonic stem cell lines maintain pluripotency and proliferative potential for prolonged periods of culture.* Dev Biol, 2000. **227**(2): p. 271-8.
50. Nair, L.S., S. Bhattacharyya, and C.T. Laurencin, *Development of novel tissue engineering scaffolds via electrospinning.* Expert Opinion on Biological Therapy, 2004. **4**(5): p. 659-668.
51. Eugene, D.B., et al., *Utilizing acid pretreatment and electrospinning to improve biocompatibility of poly(glycolic acid) for tissue engineering.* Journal of Biomedical Materials Research Part B: Applied Biomaterials, 2004. **71B**(1): p. 144-152.
52. Vasita, R. and D.S. Katti, *Nanofibers and their applications in tissue engineering.* Int J Nanomedicine, 2006. **1**(1): p. 15-30.
53. Murugan, R. and S. Ramakrishna, *Design Strategies of Tissue Engineering Scaffolds with Controlled Fiber Orientation.* Tissue Engineering, 2007. **13**(8): p. 1845-1866.
54. Larsson, I., et al., *A human neoplastic hematopoietic cell line producing a fibroblast type of interferon.* Dev Biol Stand, 1979. **42**: p. 193-7.
55. Poon, S.S. and P.M. Lansdorp, *Measurements of telomere length on individual chromosomes by image cytometry.* Methods Cell Biol, 2001. **64**: p. 69-96.
56. NordfjÃ¤ll, K., et al., *Telomere length and heredity: Indications of paternal inheritance.* Proceedings of the National Academy of Sciences of the United States of America, 2005. **102**(45): p. 16374-16378.
57. Thomas, S. and G. Johannes, *The Ki-67 protein: From the known and the unknown.* Journal of Cellular Physiology, 2000. **182**(3): p. 311-322.
58. Tang, D.D., *Intermediate filaments in smooth muscle.* Am J Physiol Cell Physiol, 2008. **294**(4): p. C869-878.
59. Hinz, B., *Formation and Function of the Myofibroblast during Tissue Repair.* J Invest Dermatol. **127**(3): p. 526-537.
60. Slijepcevic, P., *Telomere length measurement by Q-FISH.* Methods in Cell Science, 2001. **23**(1): p. 17-22.
61. Lutolf, M.P. and J.A. Hubbell, *Synthetic biomaterials as instructive extracellular microenvironments for morphogenesis in tissue engineering.* Nat Biotechnol, 2005. **23**(1): p. 47-55.
62. De Coppi, P., et al., *Isolation of amniotic stem cell lines with potential for therapy.* Nat Biotechnol, 2007. **25**(1): p. 100-6.
63. Rabkin, E., et al., *Evolution of cell phenotype and extracellular matrix in tissue-engineered heart valves during in-vitro maturation and in-vivo remodeling.* J Heart Valve Dis, 2002. **11**(3): p. 308-14; discussion 314.
64. Dror, Y., et al., *Carbon Nanotubes Embedded in Oriented Polymer Nanofibers by Electrospinning.* Langmuir, 2003. **19**(17): p. 7012-7020.
65. Ayutsede, J., et al., *Carbon Nanotube Reinforced Bombyx mori Silk Nanofibers by the Electrospinning Process.* Biomacromolecules, 2005. **7**(1): p. 208-214.
66. Supronowicz, P.R., et al., *Novel current-conducting composite substrates for exposing osteoblasts to alternating current stimulation.* Journal of Biomedical Materials Research, 2002. **59**(3): p. 499-506.

67. Okuda, K., et al., *Telomere attrition of the human abdominal aorta: relationships with age and atherosclerosis.* Atherosclerosis, 2000. **152**(2): p. 391-398.
68. Matthews, C., et al., *Vascular smooth muscle cells undergo telomere-based senescence in human atherosclerosis: effects of telomerase and oxidative stress.* Circ Res, 2006. **99**(2): p. 156-64.
69. Kurz, D.J., et al., *Chronic oxidative stress compromises telomere integrity and accelerates the onset of senescence in human endothelial cells.* J Cell Sci, 2004. **117**(11): p. 2417-2426.
70. Brown, J.W., et al., *Valved Bovine Jugular Vein Conduits for Right Ventricular Outflow Tract Reconstruction in Children: An Attractive Alternative to Pulmonary Homograft.* The Annals of Thoracic Surgery, 2006. **82**(3): p. 909-916.
71. Wells, W.J., et al., *Homograft conduit failure in infants is not due to somatic outgrowth.* Journal of Thoracic and Cardiovascular Surgery, 2002. **124**(1): p. 88-96.
72. Neves, J.P., et al., *MECHANISMS UNDERLYING DEGENERATION OF CRYOPRESERVED VASCULAR HOMOGRAFTS.* J Thorac Cardiovasc Surg, 1997. **113**(6): p. 1014-1021.
73. Hawkins, J.A., et al., *Class I and class II anti-hla antibodies after implantation of cryopreserved allograft material in pediatric patients.* The Journal of Thoracic and Cardiovascular Surgery, 2000. **119**(2): p. 324-330.

7 Table of Figures

8 Appendix

8.1 FACS dotplots Samples A (OVS1, OVJ2, OVJ3)

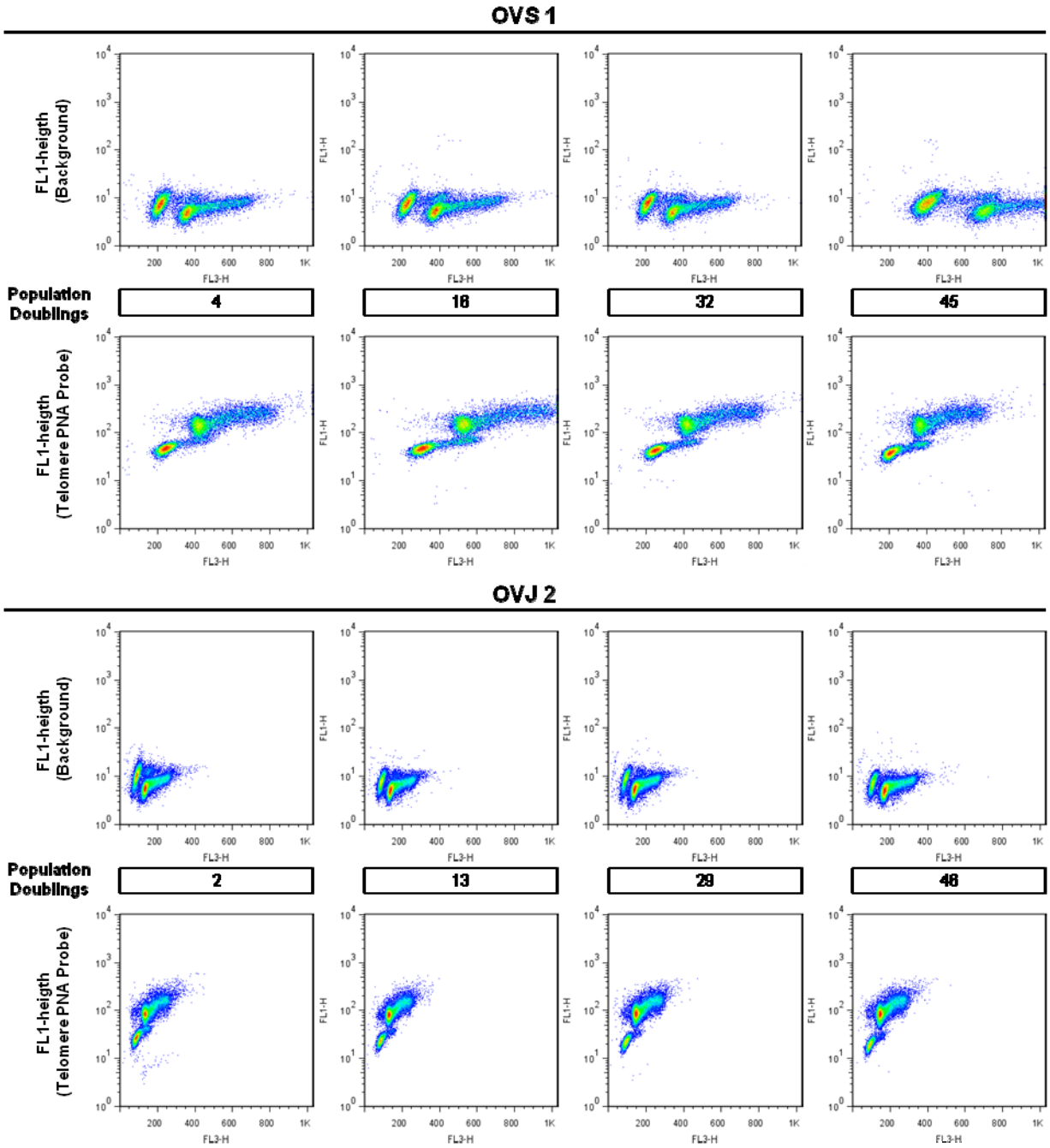

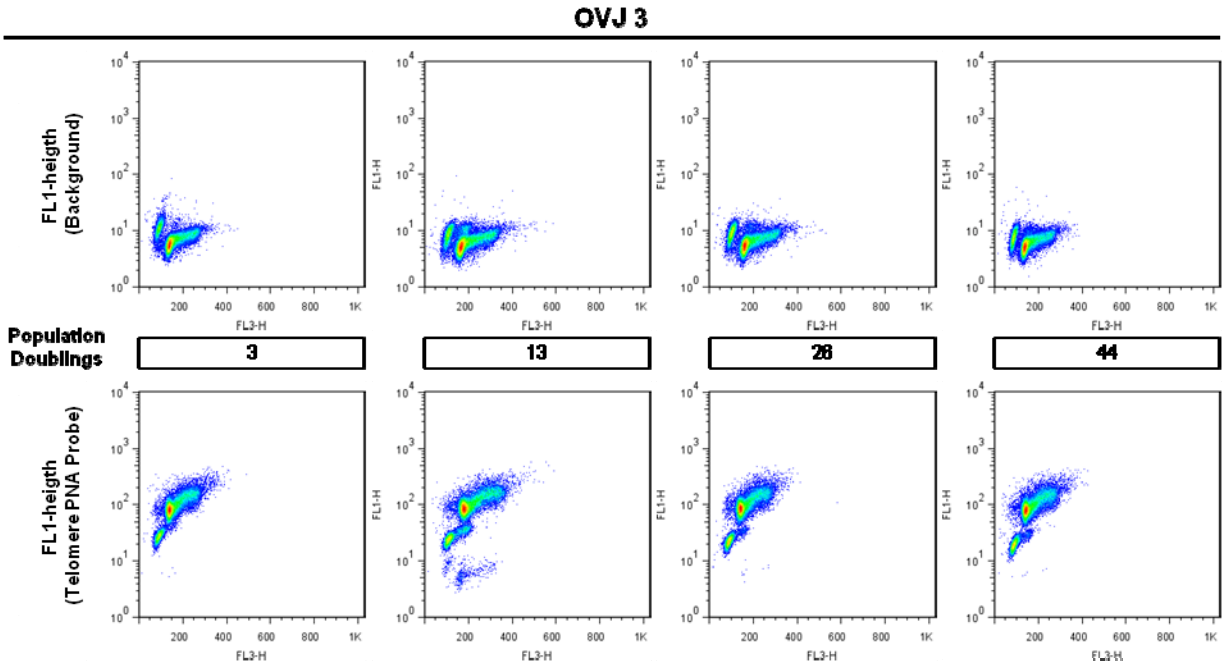
OVJ 3
FL1-heigth (Background)
FL1-heigth (Telomere PNA Probe)
Population Doublings
3
13
28
44
FL1-H
FL3-H
200
400
600
800
1K

8.2 FACS dotplots Samples B (OVS1, OVJ2, OVJ3)

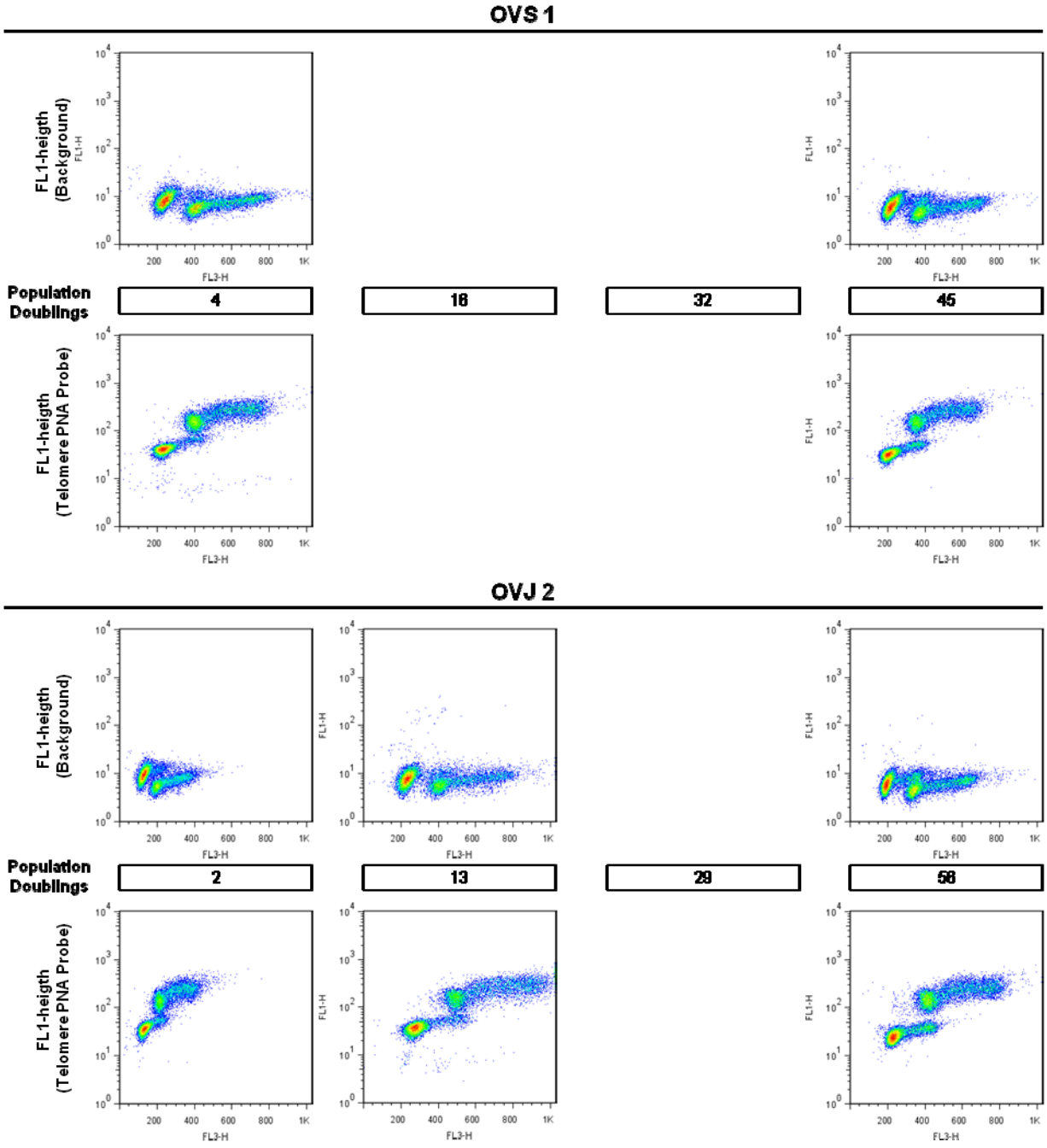

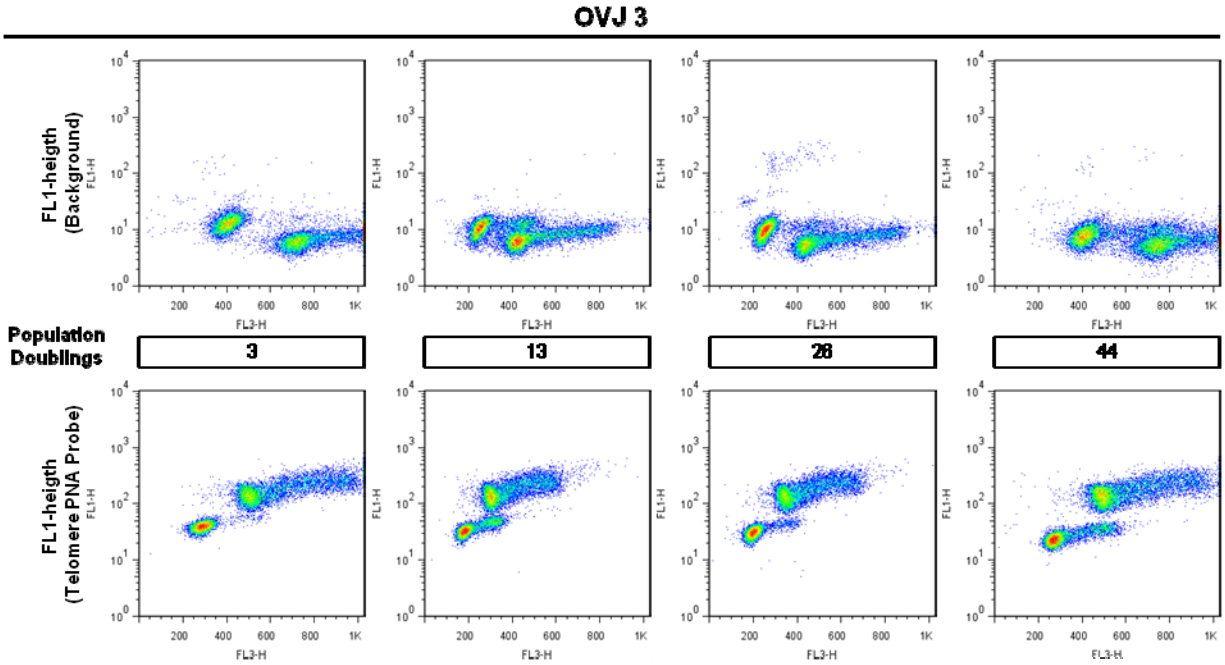
OVJ 3
FL1-heigth (Background)
FL1-heigth (Telomere PNA Probe)
FL1-H
FL3-H
200
400
600
800
1K
Population Doublings
3
13
28
44

8.3 Telomeric fluorescence: Native and TEVG

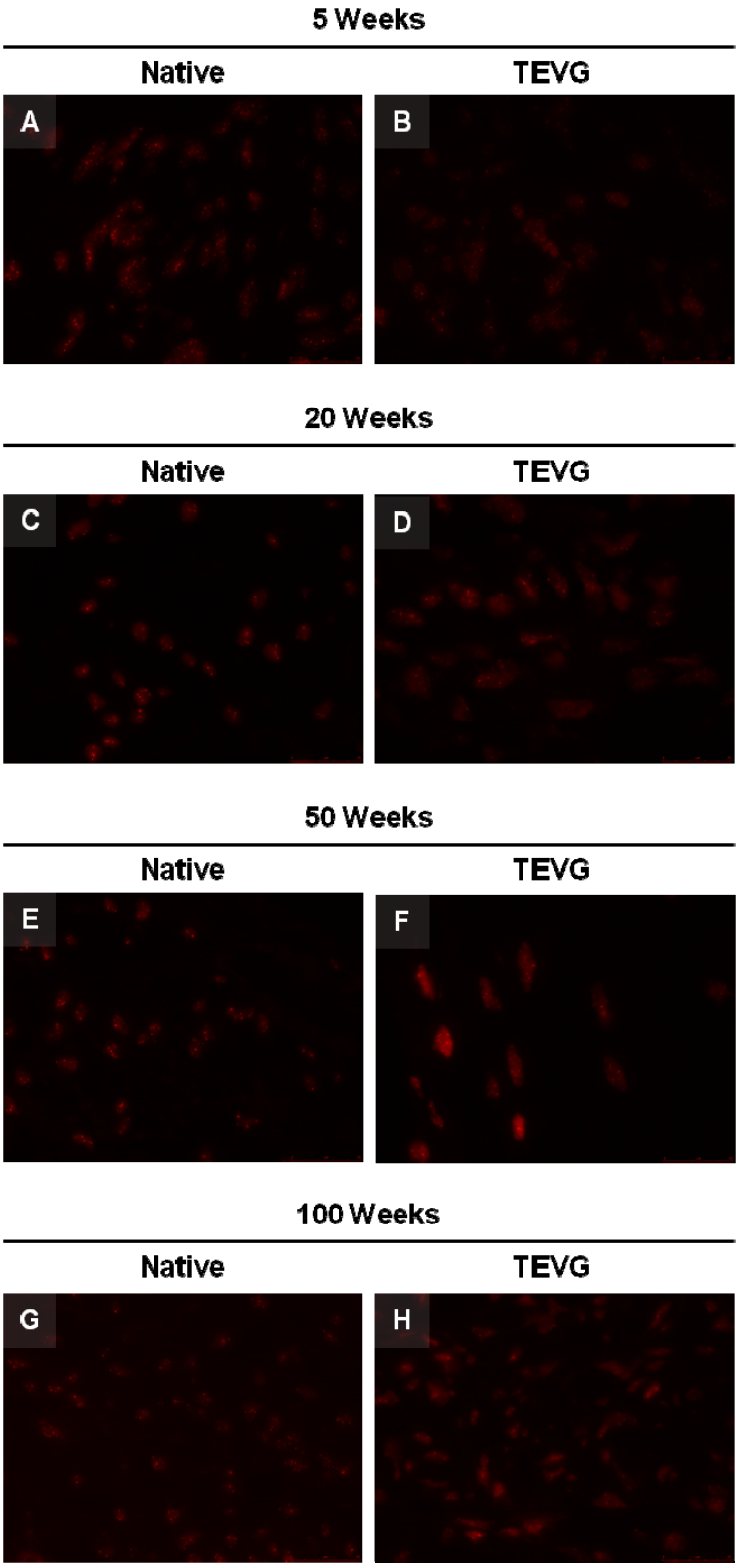

9 Acknowledgements

The author would like to thank:

- Dr. sc. nat. Jens Kelm for his patience and devotional support and his teaching in conducting state of the art scientific experiments.
- Prof. Dr. med. Simon Philipp Hoerstrup for his support and approval of this study.
- Dr. Malgorzata Kisielow, Flow Cytometry Laboratory, ETH Zurich, for her help and support on the BD FACS Calibur.
- My parents for their patience, love and support during my studies and the time thereafter.

10 Curriculum vitae

Zürcher, Armin Andreas Beat

Persönliche Information

- Staatsangehörigkeit: Schweiz
- Geburtsdatum: 14.07.1981
- Geburts- und Wohnort: Zug
- Konfession: römisch-katholisch
- Zivilstand: ledig
- Bürgergemeinde: Menzingen (ZG) und Zürich
- Eltern: Dr. med. dent. Armin und Eleonora Zürcher-Eberhard
- Geschwister: Beatrice (*1980) und Susanne (*1983)

Aus- und Fortbildung

- 1988-1994: Primarschule Stadt Zug
- 1994-2001: Kantonsschule Zug, Matura Typus C
- 1998-1999: Austauschjahr in Williams, Arizona USA
- 2001-2007: Studium der Humanmedizin, Universität Zürich

  - 1. Propädeutikum: Sommer 2002
  - 2. Propädeutikum: Sommer 2003
  - 1. Teil Staatsexamen: Sommer 2004
  - 2. und 3. Teil Staatsexamen Herbst 2007
  - United States Medical Licensing Examination (USMLE) Step 1: Nov. 2005
  - United States Medical Licensing Examination (USMLE) Step 2 CK: Feb. 2008

- 2004+2006: 15 Wochen militär-medizinische Kaderausbildung (KK med 1+2), Moudon
- 2008: Basic Science Writing Course, Zürich (Association for Research in Surgery)
- 2009+2010: Stabslehrgang + techn. Lehrgang, Armee-Ausbildungszentrum Luzern
- 2009: ACLS Providerkurs, Bern
- 2009: Abdomen-Sonographie Grundkurs, Schwyz
- 2009-2010: Assistenzarzt Innere Medizin, Spital Schwyz